Journal of Geochemical Exploration 184 (2018) 271–295

Contents lists available at ScienceDirect

Journal of Geochemical Exploration

journal homepage: www.elsevier.com/locate/gexplo

Reprint of "Vertical migration of radio-caesium derived from the Fukushima Dai-ichi Nuclear Power Plant accident in undisturbed soils of grassland and forest"☆

S. Mishra[a,b], S.K. Sahoo[a,*], P. Bossew[c], A. Sorimachi[d,e], S. Tokonami[e]

[a] National Institutes for Quantum & Radiological Science and Technology, Anagawa 4-9-1, Inage-ku, Chiba 263-8555, Japan
[b] Bhabha Atomic Research Centre, Trombay, Mumbai 400085, India
[c] German Federal Office for Radiation Protection, Köpenicker Allee 120-130, 10318 Berlin, Germany
[d] Fukushima Medical University, Hikarigaoka 1, Fukushima 960-1295, Japan
[e] Institute of Radiation Emergency Medicine, Hirosaki University, Aomori 036-8564, Japan

ARTICLE INFO

Keywords:
FDNPP
Cs radioisotopes
Vertical migration
Soil parameters
Distribution coefficient
Empirical and model-based transport parameters

ABSTRACT

The vertical distribution of radio-caesium (^{137}Cs and ^{134}Cs) in undisturbed soil profiles of grassland and forest soils, derived from the Fukushima-Daiichi Nuclear Power Plant (FDNPP) accident that occurred on 11 March 2011, was studied. Surface soil and depth profile soil samples were collected from six locations within the 20 km zone of FDNPP, during November 2012 and June 2013. The activity ratio for ^{137}Cs and ^{134}Cs was found to be almost constant about 1 within the soil profiles as well as in the surface soil, indicative of FDNPP accident origin. From soil depth profile distribution of Cs activity, it is observed that Cs is strongly bound to soil materials, which slows Cs migration. > 90% of the activity was found to be retained within the upper 5 cm layer. Retardation of Cs movement has been quantified by measuring sorption of Cs in soil in terms of distribution coefficient (K_d) using the laboratory batch method. Faster migration has been observed in case of forest land soil compared to grassland soil. The empirical migration velocity of Cs radio isotope was estimated from the depth profile Cs concentration and found to vary from 1.1 to 1.7 and 0.85 to 3.5 cm y^{-1} in grassland and forest soil, respectively. The residential half life for Cs isotopes was found to be 1.03–7.75 y and 1.18–4.67 y for grassland and forest land respectively using a compartmental model. In addition to the empirical analysis of the profiles, analytical models were fitted to the data which may help elucidate the physical nature of the transport of trace elements.

1. Introduction

Caesium radioisotopes have been released to the environment as a result of atmospheric nuclear weapon tests, leading to the so-called global fallout, and of nuclear power plant accidents. As a result, radioisotopes of caesium are deposited globally on the surface of the Earth. Deposition density of global fallout depends mainly on geographical latitude and precipitation; fallout from NPP accidents depends on emission history and on the meteorological situation during release. Actual inventories depend on local ecological processes which can lead to re-distribution of deposited Cs (Ritchie and Mc Henry, 1990; Lee and Lee, 1997; Hien et al., 2002). In contrast to global fallout from atmospheric bomb tests, the deposition of radio-caesium released during nuclear power plant accidents is regional. The Fukushima Dai-ichi Nuclear Power Plant (FDNPP) accident, in particular, resulted in strongly spatial varying deposition of caesium (Saito et al., 2015; Sanada and Torii, 2015), depending on the trajectories of air loaded with radionuclides and on precipitation during passage of the clouds.

DOI of original article: http://dx.doi.org/10.1016/j.gexplo.2016.07.023
☆ This article is a reprint of a previously published article. For citation purposes, please use the original publication details; S. Mishra et al. / Journal of Geochemical Exploration 169 (2016) 163–186.
* Corresponding author.
E-mail address: sahoo.sarata@qst.go.jp (S.K. Sahoo).

http://dx.doi.org/10.1016/j.gexplo.2016.07.027
Received 19 April 2016; Received in revised form 20 June 2016; Accepted 26 July 2016
Available online 10 November 2017
0375-6742/

The resulting contamination pattern is similarly complex to the one generated by the Chernobyl nuclear power plant accident in 1986; e.g. Izrael et al. (1996) for the regional distribution.

^{137}Cs ($T_{1/2}$ = 30.17 y) is a fission product and a beta emitter, which decays to short lived ^{137m}Ba ($T_{1/2}$ = 2.55 m) which is a gamma emitter with energy 661.6 keV, in equilibrium with ^{137}Cs in most practical situations. Therefore, in practice ^{137}Cs is often considered as gamma-emitter. Given its volatility and high fission yield, large amounts have been released, which explains its radiological importance. Among long-lived radionuclides released by any nuclear accident, radio-Cs is the radionuclide of major concern on the longer term. The radionuclide is regarded as one of the most important constituent of the worldwide fallout because 60% of the collective effective dose equivalent commitment from external radiation associated with past atmospheric nuclear weapon testing can be attributed to ^{137}Cs (UNSCEAR, 1988). It causes radiation dose to humans directly via external radiation and indirectly by root uptake of plants and transfer into human diet (Shinonaga et al., 2005). Its behaviour in soil has been extensively investigated following CNPP accident (UNSCEAR, 1988). The FDNPP accident also released ^{134}Cs ($T_{1/2}$ = 2.06 y), ^{135}Cs ($T_{1/2}$ = 2.3 My) (Zheng et al., 2014) and ^{136}Cs. The latter is of secondary radiological significance compared to ^{137}Cs since it is short lived ($T_{1/2}$ = 13.16 d). Caesium deposition in soil could be due to several ways: directly from atmosphere, wash-off from vegetation, turnover from vegetation, re-deposition of eroded soil particles and deposition from water on floodplains and coastal regions (Ritchie and Mc Henry, 1990). It is rapidly and strongly adsorbed by soil particles, especially by clay minerals (vermiculite in particular) (Tamura, 1964). The adsorption of Cs mainly occurs through an ion exchange process (Staunton et al., 2002) and also depends on the content of organic matter. Generally, in soil with high organic matter content the adsorption of Cs is reversible and it is then more available for uptake by plants (Valcke and Cremers, 1994). The adsorption of Cs is decreased by presence of competing ions of K or Na (Coleman et al., 1963). Therefore, a thorough chemical characterization of soil is important to interpret the observed migration behaviour of Cs.

Even if fully adsorbed on soil particles, Cs may be redistributed mechanically within the soil profile due to perturbation processes (Southard and Graham, 1992). Cs can also be taken up by plants and fungi which is a more complex mechanism than simple ion exchange process. Recent studies support the role of microorganisms in the retention and bioavailability of Cs in soils (Drissner et al., 1998; Stemmer et al., 2005). In agricultural field, Cs may be removed with crops by uptake from soil. Therefore, site specific conditions and environmental parameters are of paramount importance for transport and relocation of Cs isotopes deposited on the soil surface.

The migration of ^{137}Cs is a rather complicated process. Physical and chemical processes involved are advective transport and percolation with soil solution, diffusion within the soil solution, ad- and desorption to, and other chemical reactions of Cs with soil matter and biomass, and mechanical redistribution together with soil matter by erosion, bioperturbation (i.e. the activity of animals) or soil particles carried by percolating rain water. In case of anthropogenic impacted soils such as ploughed fields or landscaped terrain, additional mechanisms apply. In this paper, we restrict to undisturbed soils of natural or semi-natural environments (for the latter, typically pastures or cultivated forests). Poreba et al. (2003) gave an overview of the different processes in the environment. These processes are in turn controlled by topographic factors (inclination, relief), climatic factors (precipitation, frost period) and pedological factors (soil composition, chemistry and texture) and also controlled by biological activity (plant cover, soil biota) and erosion potential. To assess all controlling factors is nearly impossible; in addition, they are subject to horizontal and vertical heterogeneity at different length scales even in a seemingly uniform landscape. Therefore one has to restrict while describing the processes in terms of aggregated quantities (e.g. effective dispersion constant, retardation factor) or vertically or horizontally averaged quantities, which can be considered as quantities which summarize a number of processes that cannot usually be resolved easily.

The initial Cs deposition can be estimated in locations where no post-deposition relocation (e.g. erosion) can be anticipated to have occurred, and by sampling down to a sufficient depth; due to usually low mobility of Cs the inventory is mostly concentrated within the top layers (depending on time since deposition). The situation is different for comparatively highly mobile elements such as Sr, whose deposition density is often difficult to estimate from inventory after some years post deposition. Much of initial deposition must be expected to have been carried away by ground water, in many cases.

The presence of fallout ^{137}Cs in the soil results in a long-term external gamma radiation dose to humans. The dose rate depends on physical decay, inventory, but also on the vertical profile of the radionuclide in the near-surface soil layers. As the ^{137}Cs migrates to deeper layers with time, overlying soil shields the gamma rays. This effect results in a decrease of external dose rate above ground with time. For example, (Saito and Petoussi-Henss, 2014) give a dose rate conversion factor for superficial deposition equal to 3.15 (nSv h^{-1})/(kBq m^{-2}), referring to ambient equivalent dose rate. On the other hand, Bossew et al. (2001) found a factor about 1 (nSv h^{-1})/(kBq m^{-2}), for Chernobyl fallout as average over Austrian undisturbed soils about 4 to 8 years after fallout, when the ^{137}Cs had migrated typically a few cm downwards. The difference shows the efficiency of shielding by a thin soil layer only.

The internal exposure from radionuclides incorporated by ingestion of contaminated food is also affected by their vertical migration because it determines the residence time or probability of the radionuclide in soil layers relevant for the uptake by plant roots. Therefore, radionuclide migration in the soil is considered very crucial in evaluating the radiation exposure of the population (Müller and Bleher, 1997). Long-term predictions can be based on migration models whose parameters (specific to soil types) can be derived from empirical profiles. Examples are shown in this article. In any case, understanding the processes involved and modelling the migration is necessary prerequisite for predicting the long term behaviour (Bossew and Kirchner, 2004). The residence time in a soil layer and the migration velocity of a radionuclide are the basic transport parameters of the radionuclide within the soil (Müller and Bleher, 1997; Monte et al., 2003; Bossew et al., 2004; Putyrskaya and Klemt, 2007). Some authors (Frissel and Pennders, 1983; Denk and Felsmann, 1989) have therefore suggested the use of physical parameters such as residence half-times and migration rates to design dynamic models for the quantitative description of the transport processes in soil. This has also been considered in the present article.

The objective of this study is the investigation of migration properties of Cs in undisturbed soils (3 forest and 3 grassland sites) within the 20 km zone around the Fukushima Nuclear Power Plant. From the empirical ^{137}Cs depth profiles, empirical migration parameters are derived. Residence time and the migration velocity have been calculated using a compartmental model. Factors related to soil type and physico-chemical characteristic as controls of Cs mobility are discussed. Finally, in order to describe the migration process and distribution pattern the suitability of various analytical transport models is discussed.

2. Experimental

2.1. Description of sites

Soil samples were collected from six locations within 20 km from FDNPP as shown in Fig. 1. Five samples (GL-1, GL-2, GL-3, FL-2 and FL-3) are from Namie town and one sample (FL-1) from Futaba town with comparatively high ^{137}Cs inventories. Undisturbed forest and grassland soil samples lying in the direction of the radioactive plume generated by the accident with moderate to high contamination were selected for

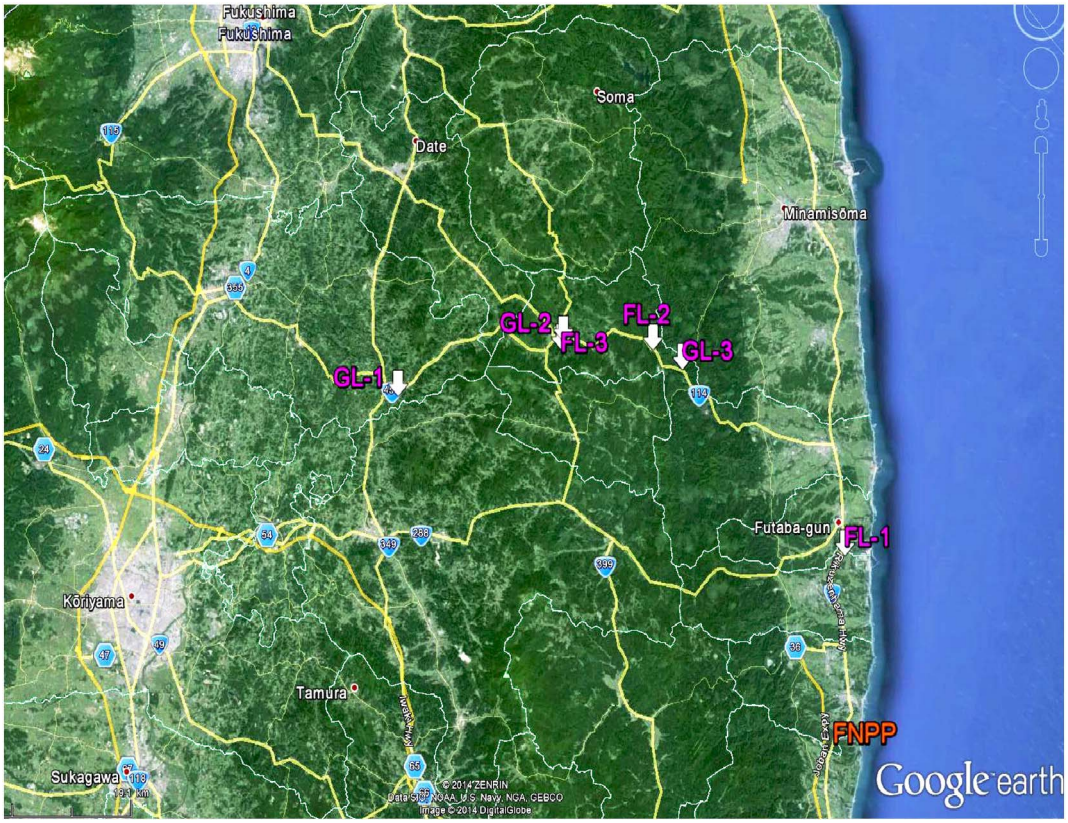

Fig. 1. Locations of the sampling sites around FDNPP.
Screen shot from Google Earth, (c) 2015 ZENRIN; data SiO NOAA US Navy NGA GEBCO; image (c) 2015 DigitalGlobe.

Table 1
Sampling locations with detailed information.

Sample location (Code)	Land use condition	Sampling date (M/D/Y)	Latitude (°)	Longitude (°)	Ambient dose rate (μSv h^{-1})	Soil core thickness (cm)
GL-1A	Grassland	11/8/2012	37.524	140.936	5	0–2, 2–4, 4–6, 6–8, 8–10, 10–15, 15–20
GL-1B	Grass field	9/26/2012	37.528	140.931	5	0–2, 2–4, 4–6, 6–8, 8–10, 10–15
GL-2A	Grass field with gravel	11/7/2012	37.558	140.753	6.5	0–2, 2–4, 4–6, 6–8, 8–10
GL-2B	Grass field with gravel (up land)	6/27/2013	37.557	140.750	6.5	0–5, 5–10, 10–15
GL-3	Grass field with gravel	6/28/2013	37.541	140.862	16.9	0–5, 5–10, 10–15, 15–20
FL-1A	Forest	11/8/2012	37.423	141.011	27.4	0–2, 2–4, 4–6, 6–8, 8–10, 10–15, 15–20
FL-1B	Forest	9/26/2012	37.422	141.011	27.4	0–2, 2–4, 4–6, 6–8, 8–13
FL-2A	Forest with dense litter	11/8/2012	37.553	140.835	20	0–2, 2–4, 4–6, 6–8, 8–10, 10–15, 15–20
FL-2B	Forest with dense litter	6/28/2013	37.553	140.834	18.8	0–5, 5–10, 10–15, 15–20
FL-3	Dense forest with porous organic soil	6/28/2013	37.553	140.751	3.2	0–5, 5–10, 10–15, 15–20

the study. Among grassland sites GL-1 is a plain site with plenty of bushes and grass near a pond. Before the accident this area was mostly used for grazing cattle. GL-2 is a plain area on the foot of a small mountain with gravel and pebbles on the surface. During rain this site can be flooded with water. GL-3 is a plain area near a house with gravels and filled with grass and shrub. FL-1 is a forest area surrounded by pine trees and on the slope of a mountain. Both FL-2 and FL-3 are surrounded by many big trees in a forest whereas FL-2 is covered with plenty of litter almost up to 10 cm whereas for FL-3 is characterized as highly porous soil.

2.2. Sample collection and processing

Soil samples were collected during November 2012 and June 2013. Composite surface soils within 0–10 cm were collected from each site. A stainless steel scoop was used to collect surface soil from five places randomly distributed within a 100 m^2 (10 m × 10 m) area of each field. Then the samples were mixed together to form a composite sample. During collection, grass was removed from the surface. Wherever litter (consisting mainly of dry tree leaves) was there - mainly in forest site (FL-2) - it was removed and soil was collected. Composite

Table 2
Standard analytical methods applied.

Parameter	Analytical method
pH	pH was measured in distilled water (IS 2720 Part No. 26)
Exchangeable cati1ons	Analysed with ICP-OES after extraction in NH_4-acetate
Cation exchange capacity (CEC_b)	Sum of exchangeable base ions
Grain size composition	Particles > 0.05 mm by sieving
Content of organic carbon (OC)	Loss of ignition at 460 °C
$CaCO_3$	IS 2720 Part No. 23
Major elements composition	XRF
Elemental concentration in solid phase	ICP-MS
Elemental concentration in liquid phase	ICP-MS
Distribution coefficient (K_d)	Laboratory Batch Method (USEPA, 1999)

samples were collected with the objective to produce more representative soil data from the particular site and were used for different soil parameter determination. Information about sampling sites with detailed description is given in Table 1. A stainless core sampler (30 cm in length, 5 cm in diameter) was used to collect ten core soil samples from the six sampling sites to a depth of 20 cm. From four sites additional core samples were collected at different time and used for comparison.

2.3. Sampling and sample processing

The sampler was thoroughly cleaned and dried before each sampling. In the laboratory core soil samples from different depth were first oven dried at 110 °C for 24 h to a constant weight to determine the bulk density, then after removing the extraneous materials such as roots, dead leaves, plants and gravel, sieved using 2 mm sieve for ^{134}Cs and ^{137}Cs analysis using gamma spectrometry. Composite surface soil samples were air-dried and after removal of extraneous materials sieved using (2 mm sieve) and were used for estimation of different soil parameters by standard procedures (Mishra et al., 2012). Sieved surface soil samples were further oven dried as core soil sample for radiocaesium analysis and further homogenized and pulverized to < 150 μm grain size, for trace and major elements analyses.

Cs concentration [both in C_m (Bq kg^{-1}) and C_v (Bq L^{-1})] for each layer is tabulated in Annex A. Care has been taken to collect the core soil samples without disturbing the surface as little as possible. Uneven surfaces and the places where lot of big grasses, bushes and shrubs existed were avoided. Core soils were taken directly from the surface in most of the cases. However in few cases e.g., GL-2B, in order to access the soil, dry grasses and dry twigs were removed from the top without disturbing the soil and then core soil was collected. In case of forest, mainly in FL-2, there were thick layer of dry leaves on the soil surface. Dry leaves were removed from the top before collecting soil samples. However, in FL-3, which is surrounded by dense forest and the soil was mixed with all sorts of organic material and found to be highly porous in nature.

2.4. Chemical characterization of soil and water

2.4.1. Determination of K_d value

The degree of radionuclide sorption on the solid phase is often quantified using the solid-liquid distribution coefficient, K_d, which can be used when making assessments of the overall mobility and likely residence times of radionuclides in soils. K_d is the ratio of the concentration of radionuclide sorbed on a specified solid phase to the radionuclide concentration in a specified liquid phase under equilibrium (Smith et al., 1995).

$$K_d = \frac{A_S\,(\mathrm{Bq/kg})}{A_L\,(\mathrm{Bq/L})} \quad (1)$$

where, A_S: activity concentration in solid phase; A_L: activity concentration in liquid phase.

A laboratory batch method was used for K_d estimation and stable Cs was added as a tracer, since soil is already contaminated with radioisotopes of Cs. The detailed procedure is given in our previous study (Mishra et al., 2012). The distribution coefficient (K_d) of Cs is highly dependent on ionic strength of water used for measurement. Therefore, we have collected ground water samples from the corresponding sites of soils (GL-2 & FL-3) to measure K_d values experimentally as close to in situ conditions as possible. Due to non-availability of ground water, river water samples close to (GL-3 & FL-2) and from other two sites (GL-1 & FL-1) pond water samples were collected for K_d estimation. The samples were filtered using 0.45 μm membrane filter and divided into two parts. One part was acidified for elemental analysis and non-acidified water was used for K_d estimation.

2.4.2. Soil parameters

Standard procedures were applied to measure various soil parameters possibly affecting the migration of Cs, summarized in Table 2. Soil parameters affecting the retention of Cs, mainly pH, exchangeable cations, cation exchange capacity (CEC), organic content (OC), $CaCO_3$ and particle size, have been measured using standard analytical procedures described in our previous studies (Mishra et al., 2014). Concentration of trace elements and major element concentrations were carried out using inductively coupled plasma mass spectrometry (ICP-MS) and X-ray fluorescence spectrometry (XRF) respectively.

2.5. Sample preparation and measurement by gamma spectrometry

Oven dried soil samples were sieved with 2 mm size and packed into plastic U-8 standard cylindrical containers (diameter = 48 mm; h = 58 mm) for γ-spectrometry. A high purity germanium detector (ORTEC GEM-100210) coupled with a 16k multi-channel analyzer (ORTEC, 7700-010) with a range 0–4000 keV and Seiko EG & G computer software Gamma Studio for gamma-ray spectral analysis has been used. The detector efficiency was determined using a 100 g multi-nuclide standard source supplied by Japan Radioisotope Association with quoted gamma energies ranging from 60 to 1333 keV and an overall uncertainty of < 5%. The results were compared with a certified soil standard IAEA-375 to check the reproducibility of the method. The counting time was varied from 10,000 s to 72,000 s depending on the activity concentration. Correction for the coincidence summation peaks of ^{134}Cs was applied. ^{137}Cs was measured using its 662 keV peak whereas ^{134}Cs concentration was derived from net peak areas of 605 keV and 796 keV gamma rays (Lee and Chung, 1991).

2.6. Descriptive statistics of the ^{137}Cs soil profiles

2.6.1. Estimation of empirical migration parameters

Define the inventory (Bq cm^{-2}) down to x cm depth in soil,

$$I(x) = \int_0^x C_v(\xi)\,d\xi = \int_0^x C_m(\xi)\ \rho(\xi)\ d\xi \quad (2)$$

ξ – depth (cm)
$C_v(\xi)$ – volumetric concentration at depth ξ (Bq cm^{-3})
$C_m(\xi)$ – gravimetric concentration at depth ξ (Bq g^{-1})
$\rho(\xi)$ – bulk density at depth ξ (g cm^{-3}).
The quantity

$$\mu(x) = \int_0^x \rho(\xi)\ d\xi \quad (3)$$

(g cm^{-2}), is the area-related mass down to depth x. Therefore, the

inventory is sometimes written

$$I(x) = \int_0^x C_m(\xi)\ d\mu(\xi) \tag{4}$$

In this notation the total inventory is written $I(\infty)$. Empirically, the inventory until the mth soil layer, whose boundaries are x_{m-1} and x_m, equals

$$I(x_m) = \sum_{i=1}^{m} C_{v,i}\ \Delta x_i \tag{5}$$

with $\Delta x_i = x_i - x_{i-1}$ the thickness of the i-th soil layer. The soil surface corresponds to $x_0 = 0$.

One can interpret $C_v(\xi)/I(\infty)$ as a probability density function (unit: cm^{-1}). Its mean equals

$$\langle x\rangle = \frac{1}{I(\infty)} \int_0^\infty \xi\ C_v(\xi)\ d\xi \tag{6}$$

which can be estimated as

$$\langle x\rangle' = \frac{1}{I(x_m)} \sum_{i=1}^{m} \frac{x_i + x_{i-1}}{2}\ C_{v,i}\ \Delta x_i \tag{7}$$

where m denotes the deepest soil layer.

In analogy the empirical variance equals $V = \langle x^2\rangle - \langle x\rangle^2$, and the *empirical migration velocity and dispersion* are

$$v_{emp} = \langle x\rangle/t, \quad D_{emp} = V/(2\ t), \tag{8}$$

with, t – the migration time (y).

Similarly, other empirical location measures are the geometrical mean depth and the median depth,

$$GMx = \exp(\langle \ln\ x\rangle), \tag{9}$$

$$x_{1/2}\ \equiv \mathrm{Med}(x): \Leftrightarrow \int_0^{\mathrm{Med}(x)} C_v(\xi)\ d\xi = \tfrac{1}{2}\ I(\infty), \tag{10}$$

the *median or half-value depth*. From this, the *median velocity* can be defined, $v_{1/2} := x_{1/2}/t$.

We shall remain with $\langle x\rangle$ and Med(x) as reference location parameters. Also other statistics such as quantile depths can be defined in analogy with standard statistics.

Finally, for profiles whose observed maximum lies on the surface, the empirical relaxation length is defined as the depths at which the values fall to 1/e of the surface (x = 0) value, respectively. For the depth, at which the concentration falls below 0.5, also the term half-value depth is used, not to be confused with the one defined above.

2.6.2. Residence half-times

The residence half time of ^{137}Cs in a soil layer is another measure of its mobility. It is specific to a soil layer and hence does not require any assumptions about vertical homogeneity. It can be estimated with a compartmental model (Boone et al., 1985; Bunzl et al., 1994; Frissel and Pennders, 1983) as discussed in Section 2.8. The model can be applied with ease because it does not require detailed information on the actual transport processes of the radionuclide in the soil such as the sorption properties, water infiltration. There is a disadvantage that only the residence times and migration velocity of the radionuclide within the soil layers can be obtained.

2.7. Analytical models for the transport of radionuclides in soils

The purpose of analytical migration models is threefold. Firstly, one wants to be able to describe a soil profile analytically as input for further calculations, e.g. dose rate above surface through photon transport models, as shown by (Saito and Petoussi-Henss, 2014).

Secondly, grounding the model on the physico-chemical processes which control migration and applying it to observed profiles, can quantify the controlling parameters such as effective advection velocity, and can thus inform about soil properties.

Thirdly, knowing the soil parameters, as material composition which control migration, the model can predict tracer concentrations at any time and at any depth in soil.

In reality, a complete model which describes any migration is not achievable, due to the complexity of processes and the horizontal and vertical heterogeneity of soil. Hence in the best case one can give average or probabilistic results applicable for certain soil types. Evidently accuracy of such predictions increases with the knowledge of relevant parameters, in turn implying investigation of an as large as possible number of empirical profiles.

Owing to the importance of modelling tracer or pollutant movement in soil, or porous media in general, literature about transport models is immense and cannot be reviewed here. Perhaps the most influential scientist in this field is Marinus Van Genuchten (Van Genuchten and Wierenga, 1976), who presented a wealth of analytical solutions of migration problems in his papers and reports since the early 1970s. An excellent monograph on soil physics and solute transport mechanism has been published by (Roth, 2012) and a few considerations can be found in IAEA (2009; p.103 ff.).

2.7.1. Semi-empirical models

Based on empirical evidence, analytical models are sometimes used which perform well but are not grounded in physical mechanisms, although they may turn out approximate solutions. These models are used for describing empirical profiles, but can in general not be used for predictive purposes, because they reflect the state of the system at a certain time, which changes with time. Perhaps the most popular is the *exponential model*, simply

$$C(z) = C(0)\exp(-\beta\ z), \tag{11}$$

C(z) is the activity concentration (Bq cm^{-3} or Bq g^{-1}) of the radionuclide at depth z (cm); C(0) and β are experimentally determined parameters, where C(0) is the (theoretical) concentration of the radionuclide at the surface and β (cm^{-1}) is the inverse of the relaxation length. ln(2)/β (unit: cm) is the half-value depth $z_{1/2}$, i.e. the depth in which the concentration equals half the one on the surface. Refinements are

$$C(z) = C(0)\exp(-\beta\ \mu(z)), \tag{12}$$

where the "linear" depth z is replaced by the mass-depth μ(z) (g cm^{-2}) - this model may better account for vertical heterogeneity of soil density; and

$$C(z) = C(0)\exp(-\beta\ z^{\alpha}), \tag{13}$$

thereafter called "expon-alpha", which can serve similar purposes. As an example of the additional empirical parameter, α (Mattsson, 1975) suggested a value of 0.75 for describing the profile in a lichen carpet.

The exponential model can well describe the situation at a given time not too long after deposition, but not the dynamics of the migration over longer periods. After longer migration times, typically after some months or few years, the physico-chemical processes involved result in the "deformation" of the shape of the profile from an exponential decaying towards a bell-shaped profile.

In a similar semi-empirical manner, this effect can be modelled by a *Gauss-type* function

$$C(z) \sim \exp[(z - vt)^2/(4Dt)], \tag{14}$$

with v and D as a priori empirical parameters, which however play the role of migration velocity and dispersion measure. In fact it turns out that this function is an approximate, and asymptotically ($t \to \infty$) correct solution of the CDE model (see below).

In analogy to the empirical profiles, also the analytical ones can be interpreted as probability distributions. Therefore, mean values and variances can be calculated. Let C(z) the model and J the total

inventory, i.e. $J = \int_{(0\ldots\infty)} C(z)\, dz$, then

$$\langle z\rangle_C = \frac{1}{J}\int_0^\infty z\ C(z)\ dz \tag{15}$$

The index C in $\langle z\rangle_C$ denotes that this is the mean depth under model C(z). From these, by dividing by migration time, actual mean (up to a given time) transport velocities and dispersions can be calculated, but one must be careful not to confuse these quantities with the physically grounded transport parameters.

As important example, for the exponential profile the mean equals $1/\beta$ and the variance $1/\beta^2$, so that the actual mean velocity and dispersion are $1/(\beta t)$ and $1/(2\beta^2 t)$, respectively.

Matsuda et al. (2015) proposed another heuristic model based on sech and cosh functions which is able to capture the "buckle" which appears in the profiles near the surface, after some time, as a result of downwards migration. The model has the benefit, in contrast to Gauss-type models, to be asymptotically falling exponential with depth.

The authors also proposed an "effective relaxation length" as measure of bulk migration, defined as the relaxation length in a hypothetical exponential profile which generates the same gamma dose rate above ground as the actual (possibly non-exponential) profile.

2.7.2. The convection–dispersion model

Perhaps the most popular among physically grounded analytical models is the convection–dispersion model. Many studies applying the convection–dispersion equation (CDE) have been reported in the literature. The deposition history is mostly approximated by pulse-like input functions, and effective values of the dispersion coefficient and convection velocity are obtained by fitting the analytical solution of the model equation to measured depth distributions of the radionuclides. Results of an extensive study analysing > 500 depth distributions measured in Austria after the Chernobyl accident have been reported by (Bossew and Kirchner, 2004). The authors also showed that the fitted parameter values are related to the physics of radionuclide transport in the soils studied and hence the convection dispersion equation can be used for predictive modelling. The evidence available today indicates that the convection–dispersion equation together with its parameters represent a physically based approach which can be applied for simulating radionuclide displacements in soils including predictive modelling.

The exact solution of the CDE with pulse like input onto the surface as initial condition reads,

$$\mathrm{CDE}\left(z, V, X\right) = J\left\{\sqrt{\frac{2}{\pi V}}\ e^{-\frac{(z-X)^2}{2V}} - \frac{X}{V}\ e^{\frac{2zX}{V}}\,\mathrm{erfc}\left(\frac{z+X}{\sqrt{2V}}\right)\right\} \tag{16}$$

with standardized parameters V = 2Dt and X = vt; z – soil depth (cm) and J – inventory (Bq cm^{-2}), t denotes migration time (y), v (cm y^{-1}) – the effective advective velocity and D ($cm^2\ y^{-1}$) – the effective dispersion constant. Radioactive decay has been omitted here as it will be in the following; it can be included by multiplying with $\exp(-\lambda\, t)$, λ the decay constant. "Effective" refers to "retardation" by sorption of the tracer onto the soil matter, described by the K_d concept, compared to "unretarded" migration of a non-sorbing (or non-reactive) tracer. The latter would be controlled by the interstitial velocity of soil solution and by the molecular diffusion constant in the solution.

For further discussion about the model the reader is referred to, e.g., (Bossew and Kirchner, 2004). The CDE model is not really realistic for short migration times, in many cases, although it can be useful to describe longer term migration. In the initial phase (shortly after input, i.e. hours–days) transport seems to be mainly controlled by percolation and mechanical transport. This results in an initial about exponential profile, which may be used as initial condition to the CDE model.

If one defines, heuristically, an exponentially decaying profile with decay parameter m (unit: cm^{-1}) as initial condition for the CDE model, the solution (somewhat cumbersome but straight forward along the line presented in (Bossew and Kirchner, 2004)) called CDE1, reads:

$$\mathrm{CDE1}\left(\begin{matrix} z, V, X, m \end{matrix}\right) = J\left\{\begin{matrix} m\ e^{m\left(X-z+\frac{mV}{2}\right)}\left(1-\frac{1}{2}\mathrm{erfc}\left(\frac{z-X}{\sqrt{2V}}-m\sqrt{\frac{V}{2}}\right)\right) \\ +\left(\frac{X}{V}+\frac{m}{2}\right)e^{m\left(X+z+\frac{mV}{2}\right)+\frac{2zX}{V}}\mathrm{erfc}\left(\frac{z+X}{\sqrt{2V}}+m\sqrt{\frac{V}{2}}\right) \\ -\frac{X}{V}e^{\frac{2zX}{V}}\mathrm{erfc}\left(\frac{z+X}{\sqrt{2V}}\right) \end{matrix}\right\}, \tag{17}$$

again assuming pulse input. This model has, to our knowledge, first and so far only been applied to Alpine soils of Austria, where it performed in general better than the simple CDE model proposed by Lettner et al. (2000). For small migration times the erfc terms become very small and only the first exponential term remains, as it should be according to the underlying concept.

A further modification consists in introduction of a fixed or non-exchangeable Cs phase which acts a sink in the model. Once Cs is fixed, no more available for migration in soil solution (only possibly by mechanical redistribution). In a previous investigation of soils of the area (Mishra et al., 2014) an unexchangeable (F5) fraction of about 97% after about 3 years after deposition has been found. Assuming a linear fixation model this corresponds to a very high fixation rate $f = 0.87\ y^{-1}$.

With same pulse-type initial condition as above, the analytical solution, "CDEfix", is

$$C_{ex} = (\mathrm{CDE})\exp(-f\ t)\ \text{ and }\ C_F(z, t) = f\int_0^t C_{ex}(z, \tau)\ e^{-f\tau}\, d\tau \tag{18}$$

where C_{ex} denotes the fractions available for exchange (liquid and solid), (CDE) the standard CDE solution and C_F the concentration in the fixed phase. One can show that with time the profile becomes again an exponential one,

$$C\left(z, t=\infty\right) = \frac{2Jf}{v(1+\gamma)}e^{\frac{vz(1-\gamma)}{2D}},\quad \gamma := \sqrt{1+\frac{4Df}{v^2}} \tag{19}$$

The most important shortcoming of this and the following model is that they assume vertically homogeneous soil, i.e. constant material parameters over the soil column. The results (model parameters by fitting) represent means of their values over the column. Even if the physical assumption about the dominant mechanisms, i.e. the structure of the model as such, is correct, heterogeneity may be such that the means over the column result in a poorly fitting theoretical profile. For the CDE-type models, means and variances are difficult to calculate analytically, and so are, therefore, mean actual migration velocity and dispersion.

2.7.3. A simple sorption model

Here the idea is not to assume the sorption equilibrium as expressed by the K_d concept, but a kinetic situation.

Consider two phases, phase 1 the solid and phase 2 the liquid ones.

The transport equation is $J = v\,C_2 - D\,C'_2$(J – flux, Bq/(s cm^2), C_2 the concentration in the liquid phase, because migration only occurs in this one, in this model, $C'_2 = \partial C_2/\partial z$), and the conservation/balance equations. For phases 1 and 2 are:

$$\begin{aligned} \dot{C}_2 &= -J - p_1 C_2 + p_2 C_1 \\ \dot{C}_1 &= p_1 C_2 - p_2 C_1 \end{aligned} \tag{20}$$

with $p_{1,2}$ - the transition probabilities (dimensions time^{-1}) between the solid (1) and liquid (2) phases which describe ad-/desorption kinetic. Here v denotes the actual velocity of the water, but not the retarded velocity as in the CDE model above. Practical units are d^{-1} for p_1 and

p_2 and cm d^{-1} for v.

The full solution of the system is very complicated (Van Genuchten and Wierenga, 1976) and almost intractable for practical purposes.

If one deals with strongly sorbing (or reactive) tracers such as Cs in the presence of clay minerals or organic matter, most of the tracer can be expected to be present in the adsorbed phase. One can then neglect, as an approximation, true diffusive transport, D = 0 (see also the remark at the end of Section 2.8). The solution, "SimpSorp", is then: $C_1(z,t) = \frac{p_1 J_0}{v} e^{-p_1 z/v - p_2(t-z/v)}\ I_0\left(\frac{2}{v}\sqrt{p_1 p_2 z(vt-z)}\right)$ (z < vt which guarantees causality)

$$C_2(z,t) = \frac{p_2 J_0}{v} e^{-p_1 z/v - p_2(t-z/v)}\ \frac{z p_1}{\sqrt{p_1 p_2 z(vt-z)}}\ I_1\left(\frac{2}{v}\sqrt{p_1 p_2 z(vt-z)}\right) \tag{21}$$

The total concentration is $C(z,t) = C_1(z,t) + C_2(z,t)$. I_0 and I_1 are the modified Bessel functions (see Annex C1).

For $p_2 = 0$ (no desorption): $C_1(z,t) = \frac{p_1 J_0}{v} e^{-p_1 z/v}$, i.e. the well-known exponential profile is reproduced. The asymptotic (large t) retarded velocity, i.e. migration velocity of the tracer and the effective dispersion parameter (not to be confused with dispersion as result of physical diffusion) equal

$$v^* = v\ p_2/p_1 \text{ and } D^* = v^2\ p_2/p_1^2 \tag{22}$$

Importantly, when t = 0, the solution is again the common exponential profile. A further approximation for practical purposes, may be assuming strong sorption and therefore small activity present in the liquid phase, or $C_2 \ll C_1$, is neglecting the term C_2.

Also for this model, calculation of mean and variance is cumbersome and perhaps analytically impossible.

2.7.4. Model fitting

Analytical models have to be fitted to the data to estimate the model parameters. Call the model $f(z,t; a_1,\ldots,a_n)$, with a_i the model parameters. The observed profile be C_i, i = 1 to n, an index counting the soil layers. In our case the time t is fixed, i.e. the time between sampling and deposition.

The general procedure is as follows. One defines a loss function $\varphi[f,C](a_1,\ldots,a_n)$ and finds a set $(a_1^0,\ldots,a_n^0)$ which minimizes this function. A common (and theoretically grounded) choice is

$$\varphi[f,\ C](a_1,\ \ldots\ldots,\ a_n) = \rightarrow \min., \sum_{i=1}^{m}\left[\frac{1}{\Delta z_i}\int_{z=z_{i-1}}^{z_i} f(z,\ t;\ a_1,\ \ldots\ldots,\ a_n)\,dz - C_i\right]^2 \tag{23}$$

i.e. the well-known Gaussian least-square (LSQ) condition which minimizes the squares of residuals. This may be approximated as

$$\varphi\left[f,\ C\right]\left(a_1,\ \ldots,a_n\right) = \sum_{i=1}^{m}\ [f(\zeta_i,\ t;\ a_1,\ \ldots\ldots,a_n) - C_i]^2 \tag{24}$$

where ζ_i denotes a reference depth, e.g. the mid-depth of a layer, $\zeta_i = (z_i + z_{i-1})/2$. m is the number of soil layers and $z_0 = 0$, the soil surface. $\Delta z_i = z_i - z_{i-1}$ is the thickness of layer number i. The first formula reported by (Bossew and Kirchner, 2004) has been used for fitting the CDE, but it was found that the error using the second, simplified one was small. If one wants to better honour small values, one may replace f and C by their logarithms. In practice we shall use φ/m instead of φ.

Fitting an exponential profile is simply done by log-transforming the C_i values and LSQ fitting a straight line in the $\log(C_i)$ vs. z_i plot. Again one commits a slight error because the accurate procedure would require nonlinear fitting.

2.7.5. Comparison of analytical models

The performances of different models fitted to the same data can be simply compared by comparing the value of the minimized loss function. However, one has to consider the following problem. By increasing the number of model parameters, one can always achieve a perfect fit. For example, three data points can always be fitted perfectly by a parabola, or polynomial of order 2; N data points can be fitted perfectly by a polynomial of degree N − 1. To counterbalance this "over-fitting problem", one can introduce a score which penalizes the number of parameters.

One theoretical quantity to achieve this is the *Akaike information criterion*, defined

$$\text{AIC: } = n\ln(\text{RSS}/n) + 2k, \tag{25}$$

with n - number of observations (here the number of soil layers), RSS - minimized residual sum of squares; here RSS/n is the quantity above called φ (see Annex C1); and k - the number of model parameters. The "best" model is the one with lowest AIC. Only different models on a given set of data (i.e. one particular profile) can be compared this way, but not different data sets (profiles). The seminal paper is reported by Akaike (1974). For small datasets (i.e. small n) it is recommended to use a stronger version, called AICc:

$$\text{AICc} = \text{AIC} + 2k(k+1)/(n-k-1) = n\ln(\text{RSS}/n) + 2k\ n/(n-k-1) \tag{26}$$

which penalizes the number of parameters even more strongly (Burnham and Anderson, 2004). For example, for n = 5 points, the additional term equals 6 and 24 for k = 2 and k = 3, respectively.

(The AIC has been introduced here in a superficial way only. The underlying theory is rather complicated. The interested reader is referred to statistical literature.)

2.8. Compartment models

Compartment models have been widely used to study radionuclide migration and geochemical behaviour in the soil (Bunzl et al., 1994; Frissel and Pennders, 1983). The model implies migration rates different for each soil layer because it is assumed that soil properties are uniform for each horizon but not vertically. A single migration rate is therefore associated with each soil horizon.

The multi-compartment model (Kirchner, 1998; Xu et al., 2005; Likar et al., 2001) assumes that the soil depth is split into a series of N horizontal layers connected by downward transport rates of the particular radionuclide being investigated. In this case, the transfer of activity A_i (Bq m^{-2}) of a particular radionuclide in the compartment i in a small time interval dt can be mathematically expressed as:

$$\frac{dA_i}{dt} = K_{i-1}A_{i-1} - K_i A_i - \lambda A_i \tag{27}$$

where, A_i is the concentration of solute in compartment i, t is time, K_i is the transport rate coefficient from compartment i to compartment i + 1 and also can be expressed as $K_i = i/\tau_i$ in which τ_i is the solute residence time in compartment i and λ is the disintegration constant of the radionuclide.

The initial conditions are given as:

$A(i = 1,\ t = 0) = A_0$

$A(i > 1,\ t = 0) = 0$

where A_0 is the deposited activity on the surface (Bq m^{-2}) due to the accidental release. A_0 is treated as instantaneous compared to the simulation period although the release and deposition takes place over a period of 10–20 days' time, i.e. a pulse-type input is assumed as discussed above.

A_0 is estimated by integrating the activity concentration over the sampled soil column and correcting for the physical decay of the radionuclide. In the present study, concentration values are integrated up to 20 cm.

For the first compartment the above equation becomes

$$\frac{dA_1}{dt} = -(\lambda + K_1)A_1 \tag{28}$$

which has the familiar solution,

Table 3
Chemical characteristics of bulk surface soil.

Sample No.	pH	OC %	$CaCO_3$ %	Ex. Ca meq 100 g^{-1}	Ex. K meq 100 g^{-1}	Ex. Mg meq 100 g^{-1}	Ex. Na meq 100 g^{-1}	CEC_b meq 100 g^{-1}	Sand %	Silt + clay %	K_d L kg^{-1}
GL-1A	6.30	8.8	2.18	13.02	1.07	3.55	0.03	17.68	90.8	10.2	325 ± 20
GL-2A	7.88	4.0	3.17	22.92	0.21	0.51	0.03	23.67	91.8	8.2	77 ± 2
GL-3	6.26	4.7	1.50	5.68	0.22	0.51	0.00	6.42	96.3	3.7	83 ± 9
FL-1A	4.25	18.0	1.21	5.13	0.46	2.40	0.11	8.10	91.8	8.18	168 ± 3
FL-2A	6.99	8.7	1.05	13.67	0.63	1.44	0.02	15.76	90.6	9.4	253 ± 16
FL-3	5.66	24.4	2.12	12.52	0.49	2.51	0.05	15.56	92.4	7.56	175 ± 16

$$A_1(t) = A_0 e^{-(\lambda + K_1)t}, \tag{29}$$

where A_0 is the initial activity (Bq m^{-2}),

For the second and deeper compartments i.e. (i = 2,…,n), the equation will have a solution,

$$A_n(t) = A_{n-1}\left[\frac{K_{n-1}}{K_n - K_{n-1})} + \frac{\lambda + K_{n-1}}{\lambda + K_n} e^{-(K_n - K_{n-1})t}\right] \tag{30}$$

Since the A_i values were determined experimentally, K_i is the only unknown parameter for each layer i. The K_i were calculated for by an iterative estimation using Mathematica software using Wolfram Alpha web page (http://www.wolframalpha.com/) to a good degree of accuracy.

The residence half-time of the radionuclide in layer i is defined (Boone et al., 1985) as

$$\tau_i = \frac{\ln(2)}{K_i} \tag{31}$$

In order to compare the values of τ obtained for soil horizons of different thicknesses L_i and depths, the ratio of τ/L (Ajayi, 2010) was also calculated. The reciprocal of this ratio can be considered as a velocity and therefore the rate of migration of the radionuclide in a given soil layer i can be expressed as

$$v_i = \frac{L_i}{\tau_i} \tag{32}$$

Kirchner (1998) has raised serious concerns about the applicability of the simple compartmental approach, as given here. One pertains to neglecting the diffusive component, which would manifest itself as "back-transport" term of type $K_{i+1} A_{i+1}$ in Eq. (27). However, for Cs transport this approximation seems allowable to us in most soils, given the usually high Peclet numbers which point to dominant advective transport. We plan to discuss the subject in more depth in the future. In any case, results derived by the approximation applied here should also be considered approximate.

3. Results and discussion

3.1. Physical and chemical properties of the soils

The six sites have been chemically characterized in our previous paper, (Mishra et al., 2014; upper 10 cm only). The soil parameters and major oxide contents are given in Tables 3 and 4. Soils in the studied area are mostly sandy in nature, therefore expect higher migration into deeper layer compared to clay soil (IAEA, 2009, 2010). This is also evident with low Cs-K_d (log $K_d \sim 2$) values in bulk soil at the investigation site compared to other Japanese soils (log $K_d \sim 3$, Ishikawa et al., 2008).

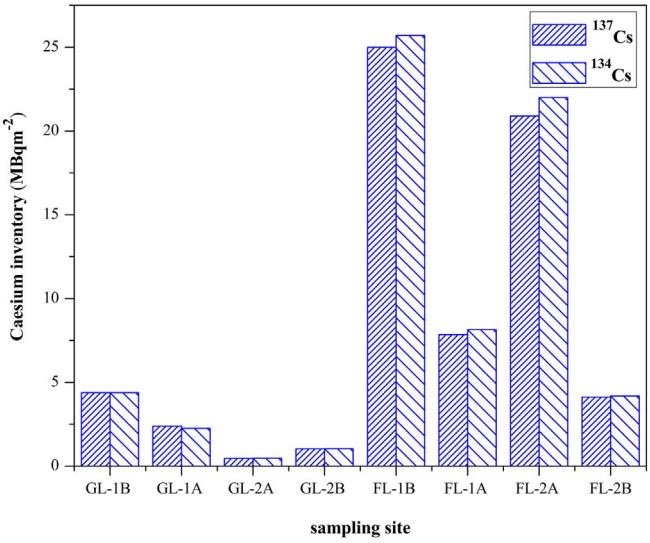

Fig. 2. Temporal variation and variation between sampling sites of ^{137}Cs and ^{134}Cs inventories in grassland and forest soil in the vicinity of FDNPP. x-Axis: sample codes, decay correction for 15th March 2011.

3.2. Radio-caesium inventories

The soil profile activity concentrations for six locations are given in Annex A. In four out of these six locations, sampling was repeated and results are coded A and B. Depth is given in cm as well as mass depth (kg m^{-2}) down to the midpoint of the depth interval. All activities are decay corrected to 15th March 2011 (the day assumed maximum deposition due to heavy rain followed by FDNPP accident on 11th March 2011).

The inventories of the soil cores found to vary from 0.46 to 25 MBq m^{-2}. This large variation was basically due to fallout

Table 4
Major oxide concentrations in bulk surface soil (mass %).

Sample No.	SiO_2	TiO_2	Al_2O_3	Fe_2O_3	MgO	CaO	Na_2O	K_2O	P_2O_5	MnO	Total
GL-1A	56.18	0.67	13.47	5.73	1.41	2.18	1.58	1.20	0.16	0.12	82.70
GL-2A	64.53	0.53	14.37	4.19	1.30	2.66	2.39	2.39	0.07	0.09	92.51
GL-3	61.96	0.46	15.53	4.25	1.15	2.27	2.70	2.26	0.09	0.09	90.75
FL-1A	51.86	0.58	14.65	4.69	0.98	0.95	1.42	1.29	0.09	0.07	76.56
FL-2A	57.44	0.50	14.89	4.69	1.45	2.28	1.97	2.11	0.01	0.09	85.43
FL-3	42.10	0.44	14.89	4.51	1.48	3.28	1.33	0.83	0.17	0.12	69.15

concentrations arising mainly from the trajectory of contaminated air and meteorological conditions, and to some degree on geography. Higher deposition was observed in the North West direction, i.e. the radioactive plume had extended into this direction. Contamination is higher in forest than in grassland. The reason may be more efficient interception of contaminated air, and retention in forest due to precipitation.

Fig. 2 shows that the differences of the measured inventories (down to 20 cm) at the same location, for two sampling dates, are considerable. It was very high for the forest site. In case of two grassland sites GL-1 and GL-2, the coefficients of variation (CV) between the results for two sampling dates are 41% and 54%, respectively. The intervals between samplings were two and seven months, respectively.

For the forest sites FL-1 and FL-2 (same intervals between samplings), we find CV's of 74% and 94%. Possible reasons for high variabilities are the following.

1. *Small-scale local variability of fallout intensity*: This phenomenon has been observed in the past (e.g. Lettner et al., 2000), and may be due to (a) locally fluctuating precipitation intensity during passage of the contaminated cloud and (b) heterogeneity of the radionuclide concentration in the passing cloud. The approximate distances between GL-1A/B, GL-2A/B, FL-1A/B and FL-2A/B were 2 m, 20 m, 1 m and 3 m, respectively. It is also known that in forests, local fallout density can vary due to variable interception and retention or accumulation of fallout by ecological processes.
2. *Redistribution post-fallout*: in the period between samplings, radiocaesium could be eroded and relocated. In particular, there are small terrain differences between GL-1A/B and GL-2A/B; GL-2A lies a bit lower than GL-2B and is sometimes flooded. Due to this fact, Cs may have been washed away from GL-2A compared to GL-2B. Particularly, combined effects of leaching and litter accumulation may lead to seemingly erratic contamination patterns in forests.
3. *Sampling effects*: In several cases, sampling was performed after heavy rain, with consequently very moist soil, which may lead to sampling errors. In the forest sites (in particular at FL-2) there is a thick litter layer, whose definition, and subsequent treatment, may be subject to humidity conditions.

The ratio of the ^{137}Cs to ^{134}Cs activity concentrations was found to be constant ≈ 1 throughout the core in all the six sites, which indicates that the origin of the radionuclides is indeed the FDNPP accident. (For comparison, the ratio of ^{134}Cs to ^{137} Cs activity concentrations for fallout from the Chernobyl accident was 0.52–0.58; for the first part of cloud reaching Sweden a ratio of 0.63 ± 0.06 was reported; variations were thought to be due to the variation in release and transport conditions, (Erlandsson et al., 1987; Devell, 1991). There is no normal ^{134}Cs/^{137}Cs ratio as 0.5. This ratio depends on the core inventory ratios in the moment of the accident influenced by the type and burning ages of the nuclear fuels. In case of Fukushima, ^{134}Cs/^{137}Cs model output from burnup calculations of the expected spent fuel inventories of the reactors (Nishihara et al., 2012) operating at the time of tsunami was found to be (~1) and compared with the ^{134}Cs/^{137}Cs ratio observed from actual sample measurement (MEXT, 2011) as well as observed in the present study. The difference of the ratios can be explained by the lower degree of enrichment used for the Chernobyl's graphite-moderated nuclear power reactor (RBMK) fuel (approximately 2%). The RBMK fuel does not allow for comparable burning ages, as in case of Fukushima's boiling water reactors (BWR) (enrichment approximately 3–4%), and will not build up a comparable amount of ^{134}Cs per ^{137}Cs by neutron activation of stable ^{133}Cs (Steinhauser et al., 2014). Considering the significant deposition of Cs activity by the FDNPP accident, the contribution from Chernobyl accident or nuclear bomb tests can be neglected in this case, at our investigation sites.

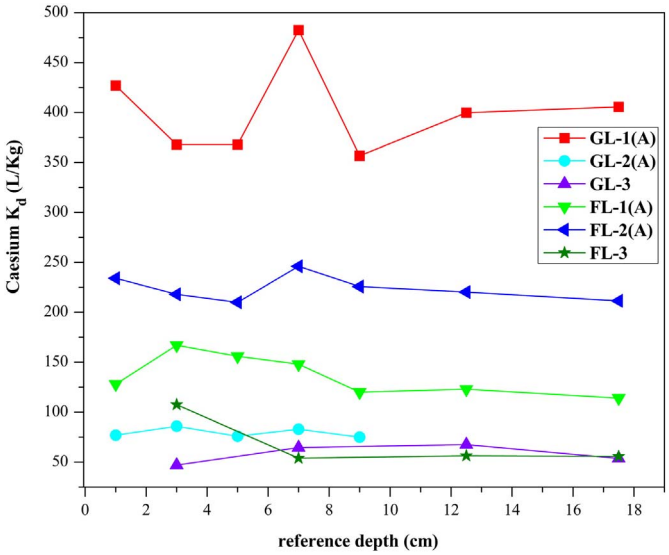

Fig. 3. Cs-K$_d$ values for different soil cores, in dependence of soil depth.

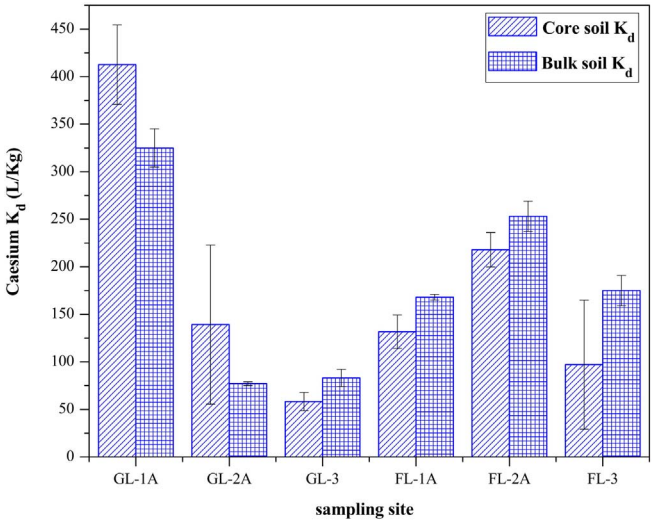

Fig. 4. Cs-K$_d$ values for core soil (average value of each layer down to 20 cm depth) and bulk soil (10 cm depth).

3.3. Effect of physico-chemical parameters of soil on vertical distribution of radio-caesium

The vertical redistribution velocity of radiocaesium in undisturbed soils is relatively low (with the exception of sandy soils and tropical laterites). The cause is fixation of caesium by the crystal lattices of clay minerals. Clay minerals are leaflike structures composed of layered negatively loaded silicate platelets. In triple layered clay minerals cations are taken up between the layers to equalize ionic charges. Caesium and potassium ions fit especially well into these interspaces due to their size and high polarity and so are fixed there (Tamura, 1964). Due to this specific binding, they are protected against leaching into deeper soil layers and are only limitedly available to plants.

In the present study, the sequential extraction of Cs in soils from these sites shows that 90% of it is bound to the silicate fraction mostly irreversibly and only 10% of it is available for exchange and migration processes (Mishra et al., 2014). K$_d$ values for bulk soil (10 cm depth) show a significant correlation ($p < 0.05$) with exchangeable K^+ ($r = 0.97$), Fe_2O_3 ($r = 0.91$) and fine particles ($r = 0.75$), whereas a reverse correlation with K_2O ($r = 0.5$) has been observed. Strong correlation of Cs-K$_d$ with exchangeable K^+ ion in soil suggests Cs sorption

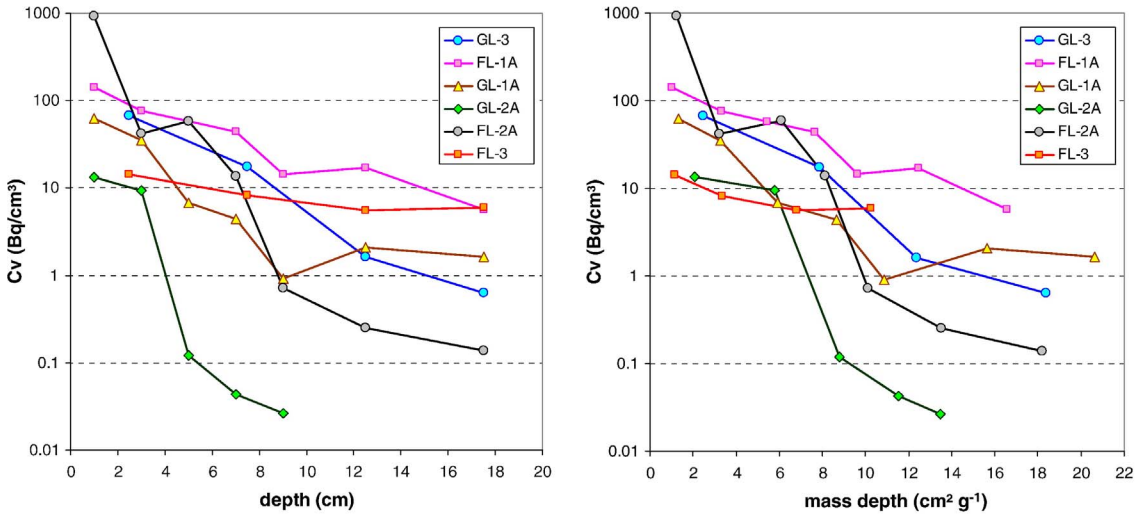

Fig. 5. Empirical profiles of ^{137}Cs in soils. Left: in dependence of soil depth; right: in dependence of mass depth.

Table 5
Empirical profile parameters. Inventory decay corrected 15th Mar. 2011.

Sample No.	t y	Inventory MBq m^{-2}	v cm y^{-1}	D cm^2 y^{-1}	$v_{1/2}$ cm y^{-1}
GL-1A	1.654	2.38	1.91	4.32	1.1
GL-1B	1.536	4.45	2.44	2.83	2.0
GL-2A	1.651	0.46	1.13	0.34	1.0
GL-2B	2.286	1.00	1.75	1.76	1.5
GL-3	2.289	4.35	1.66	1.49	1.4
FL-1A	1.654	7.84	2.90	5.86	2.1
FL-1B	1.536	25.0	1.96	3.78	0.9
FL-2A	1.654	20.9	0.85	0.48	0.7
FL-2B	2.289	4.14	1.25	0.66	1.1
FL-3	2.289	1.70	3.48	6.96	3.0

$v := \langle x \rangle / t$, $D := Var / (2t)$, $v_{1/2} := x_{1/2} / t$, "median velocity", $x_{1/2}$ – half value depth; GL – grassland, FL – forest sites.
t – migration time = time between 15th Mar. 2011 and sampling date.

was mainly controlled by ion exchange process. K^+ can efficiently compete with Cs^+ for sorption sites due to their chemical similarity, which was markedly observed in the present study with a reverse correlation with K_2O (Li et al., 2004). Significant correlation (0.84, $p \leq 0.03$) for Cs-K_d with K^+/K_2O ratio is observed. We have noticed with increase in exchangeable K^+ compared to irreversibly bound K in soil can decrease the mobility of Cs in soil by increasing Cs adsorption.

Kamel and Navratil (2002) and Lujanien et al. (2006) reported an increase in sorption of Cs with an increase in iron oxides and clay content of soil phase. This has been strongly supported by our study. We noticed positive correlation of Cs-K_d to that of Fe_2O_3 and fine particle content in soil. Japanese soils have relatively high Fe content (4.19–5.73%), thus sufficiently reduce the mobility of Cs in soil column by increasing adsorption onto Fe oxide. Litter content of soil can efficiently reduce Cs mobility by strong accumulation; this is evidenced in one of the site FL-2 where most of the Cs activity is retained within 2 cm thickness. Porosity of soil plays an important role in increasing Cs mobility. In one of our investigated sites (FL-3) higher migration is observed in soil column with high porosity (Annex A).

Table 6
Parameters of the linear fit ln(C) by z (C – volumetric concentration, z – soil depth, cm).

Sample No.	t y	β cm^{-1}	v cm y^{-1}	D cm^2 y^{-1}	r^2	p
GL-1A	1.654	0.23	2.66	5.85	0.67	0.025
GL-1B	1.563	0.28	2.31	4.19	0.96	0.00065
GL-2A	1.654	0.89	0.68	0.38	0.88	0.017
GL-2B	2.286	0.26	1.68	3.23	1.00	0.022
GL-3	2.289	0.33	1.33	2.04	0.97	0.013
FL-1A	1.654	0.19	3.20	8.47	0.94	0.00035
FL-1B	1.536	0.21	3.14	7.58	0.44	(0.22)
FL-2A	1.654	0.54	1.13	1.05	0.88	0.0017
FL-2B	2.289	0.33	1.32	1.98	0.88	(0.063)
FL-3	2.289	0.061	7.21	59.56	0.82	(0.095)

t – migration time, β = − slope; v and D according to Section 2.7.1 (end of section); p = prob (H_0: $r^2 = 0$). In brackets: not significant at 0.05 level.

3.4. Distribution coefficient and retardation factor

In a soil horizon, K_d will vary stochastically in horizontal as well as in vertical direction around a mean value. This is due to reversible sorption of the radionuclide by various soil constituents. In the field, both the hydraulic and sorption properties of a soil will vary stochastically causing serious consequences on the transport of the radionuclides in the soil (Bunzl, 2001). The horizontal random variability of K_d produces a pronounced tailing effect in the concentration depth profile of a fallout radionuclide. Kirchner (1998) showed a convective stochastic approach which takes into account spatial variability of flow and sorption and leads to a lognormal probability depth distribution of fallout radionuclides. However much less is known on the corresponding effect of the vertical random variability (Bunzl, 2002). In the present study using the bulk soil, we have measured depth wise Cs-K_d in the different soil cores at different thickness and results are given in Annex A. There was no particular trend obtained for Cs-K_d within a soil depth of 20 cm as shown in Fig. 3. However a similar trend can to some extent be observed for GL-1 and FL-2A. Due to the unavailability of data on soil parameters at different depth, there is a limitation to discuss depth variability of Cs-K_d in detail. In case of FL-3, the K_d of the upper layer was higher than the one of deeper layers. The site being highly

Table 7
Parameters of the nonlinear fit ln(C) by z_α. See header of Table 6.

Sample No.	t y	β	α	v cm y^{-1}	D cm^2 y^{-1}	r^2_{adj}	p
GL-1B	1.563	0.13	1.27	1.20	8.00	0.94	0.0061
GL-2A	1.654	1.70	0.75	0.25	0.49	0.89	(0.11)
GL-3	2.289	0.50	0.87	0.62	3.65	0.94	(0.15)
FL-1A	1.654	0.47	0.72	1.56	2.72	0.95	0.0028
FL-2A	1.654	3.84	0.43	0.16	0.34	0.90	0.0047

Table 8
Fitted CDE1 profiles.

Sample No.	v cm y^{-1}	D cm^2 y^{-1}	m cm^{-1}	φ
GL-1A	< 0.0001	< 0.0001	0.27	0.8563
GL-1B	0.28	0.87	0.31	0.0274
GL-2A	< 0.0001	< 0.0001	0.90	0.8412
GL-3	< 0.0001	0.48	0.31	0.0862
FL-2A	< 0.001	< 0.001	0.62	1.40

φ - RSS of logs.

Table 9
Fitted SimpSorp profiles.

Sample No.	v cm d^{-1}	p_1 d^{-1}	p_2 d^{-1}	v* cm y^{-1}	D* cm^2 y^{-1}	φ
GL-1A	4.98	1.40	< 1e − 4	0.127	0.444	0.8594
GL-1B	1.57	0.817	1.673	1.184	2.296	0.0367
GL-2A	5.31	5.08	< 1e − 4	0.038	0.040	0.8442
GL-3	4.55	1.57	< 1e − 4	0.106	0.306	0.0899
FL-2A	5.57	3.63	< 1e − 4	0.056	0.086	1.414

φ - RSS of logs.

porous, low K_d has been observed in the deeper layer. However, the higher K_d value on the upper layer of this site (being a forest soil, organic content 24.4% for 10 cm depth) may be attributable to organic/humic acid content.

The spatial variation of Cs-K_d has already been explained with respect to bulk soil parameters in the previous section. Fig. 4 shows a comparison between core soil Cs-K_d (K_d values for each layer is averaged over 20 cm depth) to that of composite bulk soil (down to 10 cm). Cs-K_d with similar order of magnitude was observed for the six sites when compared with core as well as bulk soil. Higher Cs-K_d uncertainty was noticed in the core samples compared to bulk soil in case of GL-2 and FL-3. GL-2 basically represents the average K_d for two soil cores (GL-2A and GL-2B). GL-2A lies in the downside of the mountains compared to GL-2B and mostly flooded with water during rainy season. This is why, a difference of one order of magnitude in Cs-K_d values between these two sites has been observed, although are located very close to each other (Annex A).

The retardation factor is defined as $R_d = 1 + K_d (\rho/\theta)$, calculated from K_d, porosity (θ) and bulk density (ρ) for each layer in different cores also given in Annex A. Significant special variation observed for R_d. can be attributed to variation in soil characteristics, which is already explained in case of K_d. However, no specific vertical distribution trend is observed for R_d at different depth in a soil core.

3.5. Empirical profiles and migration parameters

The profiles are shown in Fig. 5 as plots of the volumetric concentration (Bq cm^{-3}) against depth (cm) and mass depth (g cm^{-2}). As depth values the midpoints of the layers and the mass depths until that midpoint were defined.

The empirical migration parameters given in Table 5 were calculated from the measured depth profile concentrations according to

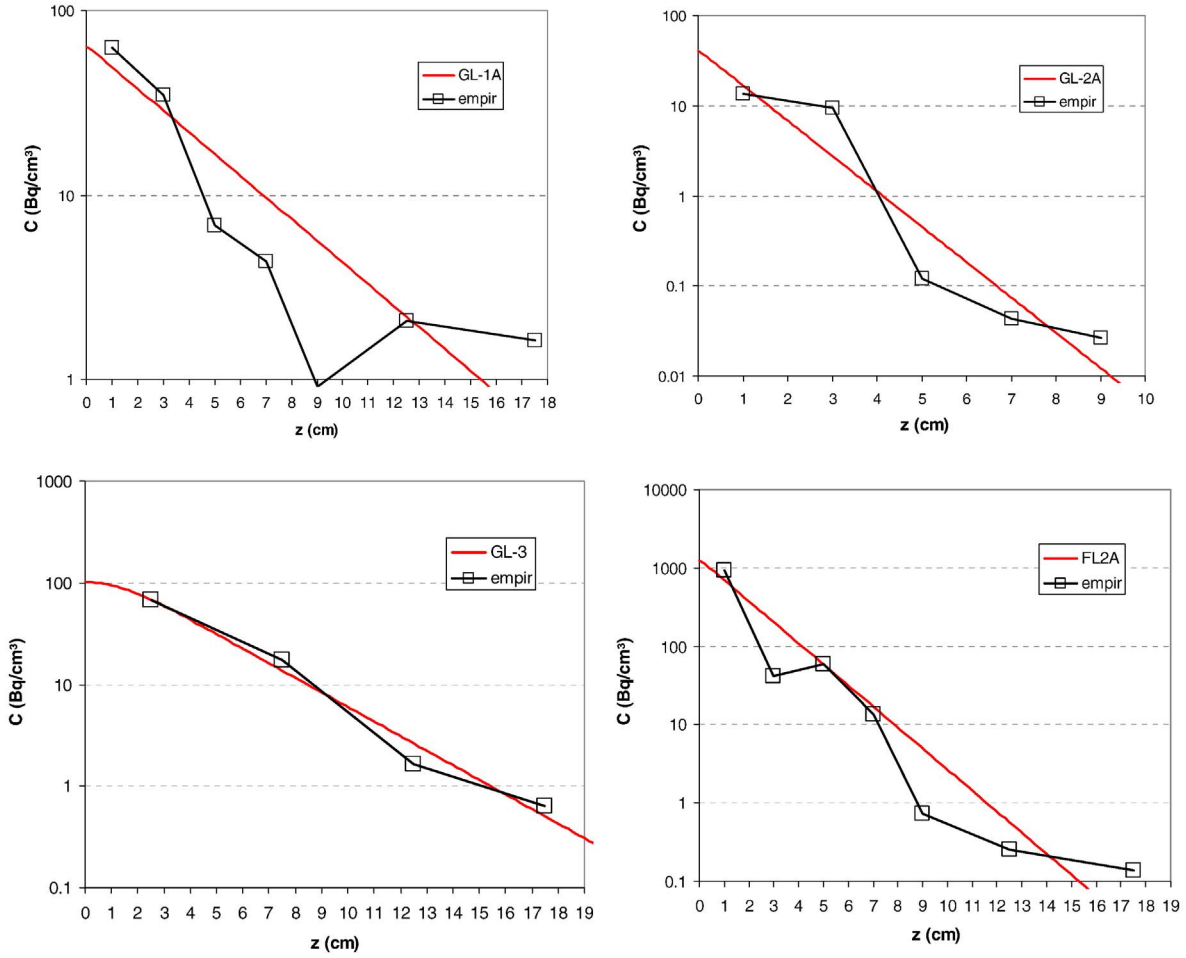

Fig. 6. Empirical and fitted profiles, CDE1 model. An additional graph (profile GL-1B) is shown in the Annex C.2, Fig. C1.

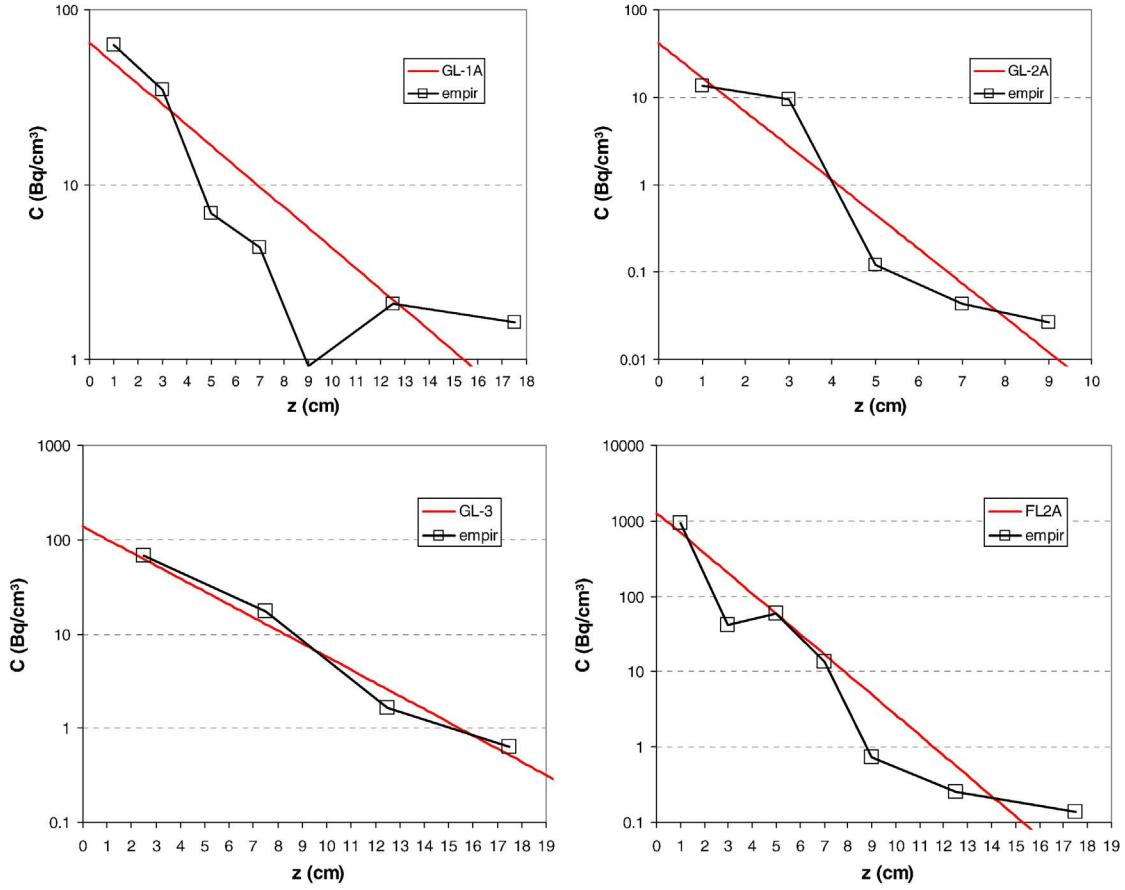

Fig. 7. Empirical and fitted profiles, SimpSorp model. An additional graph (profile GL-1B) is shown in the Annex C.4, Fig. C4.

Table 10
Migration velocities of ^{137}Cs in nine soil profiles at the six locations using compartmental model.

Sample No.	GL-1A	GL-1B	GL-2A	GL-2B	GL-3	FL-1A	FL-1B	FL-2A	FL-3
t (y)	1.654	1.536	1.654	2.286	2.289	1.654	1.536	1.654	2.289
v (cm y^{-1})	1.5 ± 0.77	2.43 ± 1.19	0.87 ± 0.01	0.73 ± 0.01	0.65 ± 0.01	2.42 ± 1.24	0.86 ± 0.45	0.87 ± 0.57	2.56 ± 0.01

t – time from deposition. v – migration velocity (cm y^{-1}).

Section 2.6. For the half value depth linear interpolation of the segments which cross half the initial value was performed.

Empirical apparent migration velocities (v, cm y^{-1}) and dispersion coefficients (D, $cm^2\ y^{-1}$) were calculated from the observed depth profile concentrations in the six sites. The values for v found to vary from 0.85 to 3.48 cm y^{-1}.

The arithmetical mean empirical velocity over all 8 profiles equals 1.93 cm y^{-1} (coefficient of variation CV = 85%), the mean empirical dispersion, 2.85 $cm^2\ y^{-1}$ (82%). Grassland sites seem to have lower velocity and dispersion than forest sites but the difference is not significant. At GL-1, GL-2, FL-1 and FL-2 two samples each were taken (A and B). It is difficult to draw conclusions from 2 samples but in tendency the dispersion (measured as GSD which is less biased than the SD and CV) appears to be lower in grassland than in forest (GSD = 1.6 and 1.7 for the grassland vs. 2.3 and 3.1 for the forest sites). This conclusion would have to be confirmed by more samples taken in small vicinity, at each site. If true, the finding would be no surprise because the comparatively high spatial variability of fallout in forest, compared to grassland, is well known. The reason is the more heterogeneous physical conditions in forest.

We want to stress again that these empirical values represent a snap shot of the migration situation at the time of sampling, but not temporally constant model parameters. It is therefore difficult to compare them with results derived from fitting models.

3.6. The exponential and Gauss-type distribution models

From Fig. 5 one can recognize that the exponential model is a reasonable approximation only for two or three of the 6 profiles. For GL-3, FL-1A and FL-3 we find calculated half-value depths of 6.1 cm, 3.7 cm and 11.4 cm, respectively. However, formally, the fit can always be performed. The results of linear regression ln(C) by z (z – mean depth of a soil layer) are given in Table 6. Further, we fitted the "expon-alpha" model $C(z) \sim \exp(-\beta\ z^{\alpha})$ as described in Section 2.7.1, Table 7 (Software used: Sigma plot 10.0.). In some cases the fitting algorithm did not converge and no results are given. For four out the five fitted profiles the α parameter is below unity, reflecting the upward-bent (convex) shape – in tendency - of the profiles. It is however difficult to say

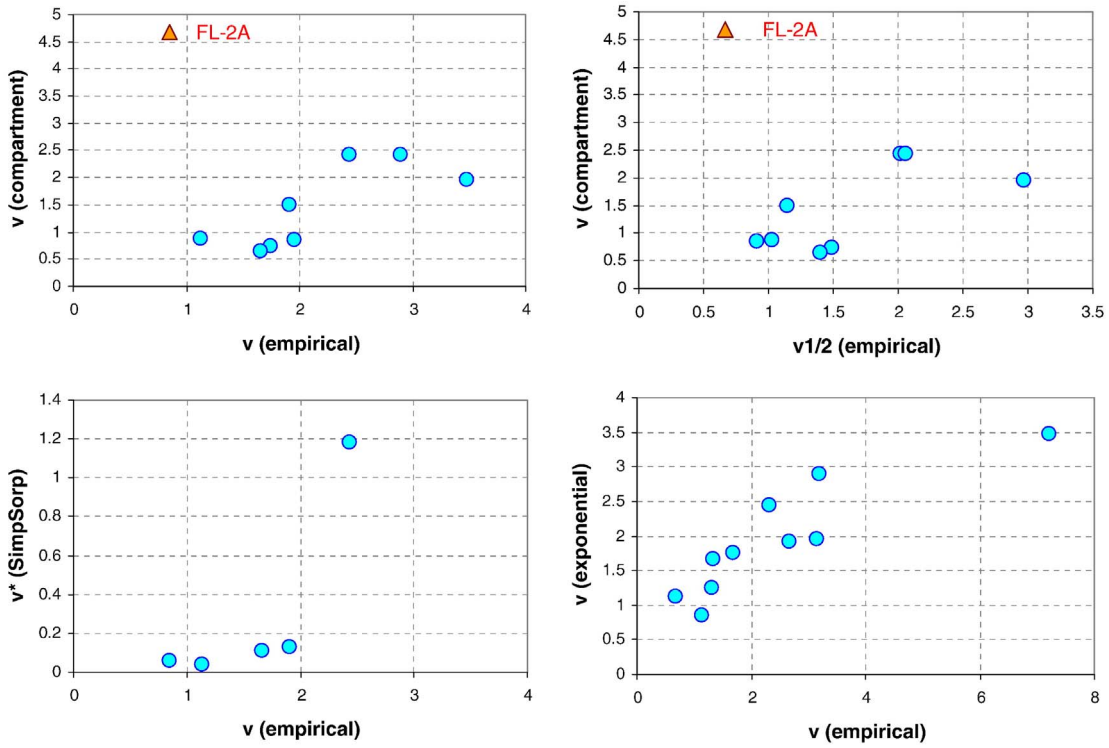

Fig. 8. Scatter plots to compare migration velocities derived from different concepts of velocity. v(empirical) = ⟨x⟩ / t, $v_{1/2}$(empirical) = $x_{1/2}$ / t. FL-2A appears as outlier.

Table 11
Pearson correlation coefficients table for soil parameters and migration parameters.

Correlation	v (EC)	D (EC)	v (CM)
pH	− 0.79[a]	− 0.81[a]	− 0.66
OC	**0.90**[*]	**0.90**[*]	0.61
$CaCO_3$	− 0.08	− 0.12	0.00
Ex. Ca	− 0.45	− 0.43	− 0.14
Ex. K	0.06	− 0.45	− 0.15
Ex. Mg	0.55	0.75[a]	0.60
Ex. Na	0.64	0.89	**0.96**[**]
CECb	− 0.34	0.67	− 0.01
Sand	0.08	− 0.11	− 0.51
Silt + clay	− 0.09	0.13	0.49
K_d	0.02	0.27	0.22
SiO_2	− **0.87**[*]	− **0.89**[*]	− 0.49
TiO_2	− 0.10	0.13	0.49
Al_2O_3	0.04	− 0.18	− 0.45
Fe_2O_3	0.08	0.33	0.31
MgO	− 0.15	− 0.07	− 0.36
CaO	− 0.01	− 0.09	− 0.52
Na_2O	− 0.72	− **0.85**[*]	− 0.78[a]
K_2O	− **0.86**[*]	− **0.96**[**]	− 0.64
P_2O_5	0.73[a]	0.77[a]	0.31
MnO	0.24	0.33	− 0.18
Bulk density	− 0.76[a]	− 0.72[a]	− 0.14
Porosity	0.80[a]	0.77[a]	0.23

EC: empirical calculation from depth profile of Cs concentration; CM: applying the compartmental model on depth profile Cs concentration; v - migration velocity (cm y^{-1}); D - dispersion coefficient (cm^2 y^{-1}). Significant correlations (prob(H0: r = 0) < 0.05) printed bold.

[**] $p \leq 0.01$.

[*] $p \leq 0.05$.

[a] $p \leq 0.1$

whether this points to a systematic effect; this would require investigating more samples. For calculating v and D, numerical integration of ∫ z C(z) dz, etc., has been performed.

For the Gauss-type model the profiles would have to appear as falling parabolas in the log(C_v) plots, Fig. 5. Evidently this is not the case for any profile, therefore this was not further investigated.

3.7. The CDE type models

The CDE model is very similar to the Gauss-type one for small migration times because then the erfc-term is almost negligible. Therefore it also requires the empirical profiles to appear as falling parabolas in plots, Fig. 5, approximately.

Since this is not the case, we should also discard this model. As a consequence of the transport mechanism on which the CDE is based, appears not to be the dominant one for these profiles. We therefore tried the CDE1 model.

For five profiles a CDE1 fit appeared technically feasible. The results are given in Table 8. That computation is feasible does not say that the model is correct, of course. The results are graphically shown in Fig. 6. The dominant contribution is the exponentially falling term (except in profile GL-1B, Annex C, Fig. C1), whereas the CDE-type modifications of the exponentials (straight lines in the log plot) do not appear to contribute consistently. Altogether the fits are poor and the applicability of the model should be doubted.

The depth range where the typical diffusion “buckle” should show is the one close to the surface. Given the rather coarse depth resolution of the profiles in that range, an effect that would be able to validate the CDE1 model cannot be observed. Also, the “beautiful” CDE1 profile of GL-1B while representing a good fit, is not convincingly supported by the observations, see Fig. C1.

Table 12
Comparison of models in terms of φ = RSS/n (RSS – residual sum of squares) and the extended Akaike criterion AICc (Section 2.7.5).

Profile	n	CDE1		SimpSorp		Expon		Expon-alpha	
		φ	AICc	φ	AICc	φ	AICc	φ	AICc
GL-1A	7	0.856	12.91	0.8594	12.94	0.71668	4.67	n.a.	n.a.
GL-1B	6	0.027	− 3.58	0.0367	− 1.83	0.04767	− 10.26	0.04	− 1.51
GL-2A	5	0.841	29.14	0.8442	29.15	0.84003	9.13	0.8	28.86
GL-3	4	0.0806	n.a.	0.0899	n.a.	0.0864	6.20	0.08	n.a.
FL-2A	7	1.4	16.36	1.414	16.42	1.073	7.49	0.62	10.67

n – number of data points per profile. n.a. – fit could not be performed.

The CDE model including a fixed phase ("CDEfix") did not yield satisfying results and was therefore not further evaluated. Discussion can be found in the Annex C on the example of profile GL-1B.

3.8. The simple sorption model

To the same five profiles as above the "simple sorption" profile was fitted. The results can be found in Table 9 and visualized in Fig. 7. Only in one case (GL-1B, further discussed in Annex C.4), a desorption rate > 0.0001 d^{-1} could be defined, so that the fitted results are of exponential shape.

3.9. Compartment models

The migration parameters mean (over layers) residence half times (τ) and migration velocities (v) of ^{137}Cs in nine soil profiles at the six locations derived from the compartmental model are given in Table 10, were calculated from the measured depth profile concentrations according to Section 2.8. The values for v found to vary from 0.65 to 2.56 cm y^{-1}. The residence half times varies from 1.03 to 7.75 years for the 9 profiles.

The arithmetical mean migration velocity over all 9 profiles equals 1.43 cm y^{-1} (coefficient of variation CV = 57%), the mean residential half times, are mentioned in Annex A. Grassland sites seem to have lower velocity (1.23 cm y^{-1}, averaged for 5 profiles) than forest sites (1.68 cm y^{-1}, averaged for 4 profiles), and similar trend also been observed, obtained in case of empirical migration velocity discussed in Section 3.6.

4. Discussion

4.1. Comparisons of migration parameters derived from different models

A number of methods have been presented to derive quantities which characterize the migration behaviour of Cs in the soil column. However, even by dimension being velocities (cm y^{-1}) or dispersions (cm^2 y^{-1}), they denote different quantities, conceptually, which must not be confused. On the example of migration velocity, these concepts are:

1. *Actually observed or empirical mean velocity* at time t: $\langle x \rangle / t$ or $x_{1/2}/t$ (Section 2.6.1);
2. *Means derived from a model*, such as the from the compartment model (Section 2.8), $v = AM(L_i/\tau_i)$ (mean over the layers i), $\langle z \rangle_{expon}/t$ or $\langle z \rangle_{CDE1}/t$ (Section 2.7.1);
3. *Model parameters*, such as the v which appears in the formula for the model CDE1 (Section 2.7.2) or derived parameters, such as the asymptotic $v^* = v\ p_2/p_1$ of the SimpSorp model (Section 2.7.3).

Although the resulting quantities are all called velocity, they denote different things as they correspond to different notions of velocity. Therefore, they are difficult to compare and one cannot say that one is correct and another one is wrong. (Of course, apart from conceptual differences, they are all affected, to different extent, by uncertainty because they are estimated from finite and uncertain data.) The differences may be compared with the one between phase and group velocity in wave theory. The former would correspond to the model parameters, the latter to the means derived from models or the empirical means. The model parameters inform about the physical nature of the investigated phenomenon, while the means measure the velocity with which the bulk of Cs actually migrates. (1) and (2) may therefore be called "bulk velocities".

It is still instructive to compare the results, e.g. as scatter plots, to visualize the discrepancies, Fig. 8.

Fair correlation is observed only for the empirical velocity vs. the one derived from the exponential distribution, lower-right graph. In concept, these velocities are defined in the same way, namely over the mean depth, $\int z\, C(z)\, dz$; C(z) stands for the empirical profile in the first, and for the fitted exponential profile in the second case. The correlation is therefore no great surprise.

4.2. Relation between migration parameters and soil characteristics

The correlation among various soil parameters with migration velocity calculated empirically from depth profile caesium activity concentration and application of compartment model is given in Table 11.

The migration velocity of Cs increased with increasing organic matter content, this is evident from the significant positive correlation of Cs migration with organic content of soil. Spatial distribution of organic substances around clay particles prevents Cs^+ adsorption due to ion exchange. Therefore subsequent fixation of Cs^+ on the clay minerals is hindered, and a weak interaction of Cs^+ with organic substances exist (Fredriksson et al., 1966) and thereby facilitates Cs migration. The adsorption of organic matters with cations on clay minerals takes place by cationic exchange at the clay-solution (Mortland, 1970). Thus the organic matter would have a tendency to maintain Cs under exchangeable form. However, Evans and Dekker, 1967 observed positive as well as negative effects of the soil organic matter content on the transfer of Cs. These differences could be explained by different proportions of organic matter components (humic acid, fulvic acid) and/or by different percentages of labile and stabile organic substances. Staunton et al. (2002) showed that the nature of the

organic matter and its interaction with mineral surfaces are as important as the amount present. However, a lot of uncertainties remain on the structure of organic matter (state of evolution) and is beyond the scope of the present study.

Significant negative correlation was observed for oxides of Si, Na and K with migration velocity, which indicates Cs sorption on silicate minerals. These oxides also show significant correlation with one another, shown in Annex B. Francis and Brinkley, 1976 and Cornell (1993) proposed two major types of Cs sorption: (1) ion-exchange with hydrated cations on planar sites of expandable phyllosilicates, and (2) selective sorption to the frayed edge sites of non-expandable phyllosilicates (micas) and interlayer sites of vermiculites. Sodium at high concentrations has been found to effectively compete with Cs for planar as well as frayed edge sites (Zachara et al., 2002).

Weak positive correlation of Cs mobility was observed with phosphorous content of soil (P_2O_5). Phosphorus availability in soil is mainly controlled by soil pH and amount of organic matter, and may be due to fertilizer phosphorus in agricultural land. Soil pH reduces Cs migration (weak correlation). Since Cs sorption in soil is mainly dominated by ion exchange on clay surface, lower pH favours protonation on the clay sites and thereby reduces Cs sorption by ion exchange. Therefore, higher pH favours sorption with decrease of Cs mobility.

Moderate correlation ($0.1 > p \geq 0.05$) has been observed between empirical migration velocity and dispersion, pH, porosity and bulk density. Correlation with porosity may be related to higher probability of percolation of rain water in more porous media. This will facilitate migration of Cs ions in soluble form or associated with very fine particulate form.

4.3. Performance and comparison of fits of analytical models

The performance of models can be compared by means of the residual sum of squares (RSS) or better, taking into account the number of model parameters, the Akaike criterion AICc (Section 2.7.5). The number of parameters is 3 for CDE1, SimpSorp and "expon-alpha" and 2 for the exponential model. The results are shown in Table 12.

We recognize that from the physically based models, CDE1 performs marginally better than SimpSorp (lower AICc). The empirical or descriptive models "expon" and "expon-alpha" have similar $\varphi = RSS/n$ but better AICc (except the "expon-alpha" model for GL-1B). For the exponential model this is because it has one parameter less.

The relatively poor performance of the physics based models can probably be explained with the low depth resolution of the profiles in the upper few cm, where the profile shape strongly depends on the transport mechanism.

4.4. Comparisons with post-Fukushima literature results

Kato et al. (2012) report results from a soil profile taken in April 2011, i.e. shortly after the accident. The profile layers are very finely resolved (0.5 cm) down to 5 cm, and with thickness 1 cm in 2 cm in greater depths. The profiles could very accurately be described as falling exponential, with relaxation length (ρ/β in our notation) 0.91 g cm^{-2} for radiocaesium, which corresponds 0.91 cm assuming $\rho = 1$ g cm^{-3}. (The authors give the actual bulk densities per depth in Annex A). The result shows that there is an initial very fast migration which cannot be explained by mechanisms of the CDE model. This justifies the assumption underlying the CDE1 model (exponential profile as initial condition) and also corroborates the rationale of the SimpSorp model.

Teramage et al. (2014) investigated a profile taken in coniferous forest soil in January 2012, more than half of Fukushima-derived radiocaesium was contained in the organic surface layers (Oh and Of), and still one quarter of pre-Fukushima (global fallout) ^{137}Cs. The Cs inventory of these layers is still fed by litter fall (contaminated needles and other parts of vegetation), but also seems to have a high retention and storage capacity for radiocaesium. To some degree, one can assume that it serves as a feeder for the underlying soil. The authors found that the profiles below the litter layers can be described as exponential; however one can see the "buckle" in the first few cm, which is a typical manifestation of downward migration with higher rate than the one through eventual feeding by the overlaying litter layer.

Takahashi et al. (2015) sampled soil cores in 4 sampling campaigns between summer 2011 and late 2012. As locations, different typical environments were chosen, such as pasture, farmland and different type of forest. In forest soil, more than half of the radiocaesium inventory was contained in the litter layer, but also on meadows the respective fraction in the plant layer was quite high in some cases. The profiles were fitted with an exponential model, yielding relaxation lengths between 0.5 and 4 cm, increasing with time, in tendency, from typically 1 to 1.4 cm. However, in many of the profiles one can visually recognize the typical migration "buckle", as deviation from the exponential function (or straight line in the log-plots, as shown by the authors).

Matsuda et al. (2015) observed that with time after fallout, profiles increasingly deviate from exponential shape. Samples were taken at > 80 locations in the Fukushima zone, if possible on apparently undisturbed soil in open land. The authors successfully fitted a heuristic model based on sech and cosh functions which accounts well for this deviation. Increasing with sampling time from Dec. 2012 to Dec. 2013, the authors found typical relaxation mass depths (ρ/β in our notation) from roughly 1.1 to 1.5 g cm^{-2}. This clearly indicates the presence of continuing downwards migration as function of migration time.

All authors find relaxation lengths much lower than we did (Table 6), with $1/\beta$ from 5 to 16 cm. This is in contrast to Matsuda et al. (2015) whose soils were sampled about the same time. The reason may be found in different soil types.

The radioceasium inventories shown in the supplementary table of Matsuda et al. (2015) show small-scale variability within few 10 m, but in general to a much lesser degree as found in our study.

Notably all authors applied much finer division of soil cores than we could achieve in our study (0.5 cm near the surface compared to 2 cm in our case), which largely facilitates profile modelling and drawing conclusions about the migration behaviour.

5. Conclusions

5.1. Empirical profiles

^{137}Cs inventories and empirical transport parameters were determined for ten soil profiles from six locations in the Fukushima zone. The inventories are very different also between closely neighbouring spots (< 1 m apart in case of forest land). The samples from closely adjacent spots were taken at different times, but it appears unlikely that redistribution processes that occurred in the mean time, could have caused the large observed differences. Whether this is a real or a sampling effect has to be checked in a future sampling campaign.

Some profile show an increase of activity concentrations at lower layers, instead of the expected monotonous decrease. This is unusual and unexpected and may point to a sampling effect, but also other possibilities with physical reasons related to soil properties must be

investigated.

Empirical migration velocities were found between 0.9 and 3.5 cm y^{-1} with perhaps (not statistically significant) somewhat slower migration in grassland than in forest soil.

5.2. K_d values

Soil characteristics, including among others texture and composition, have a distinct influence on the migration behaviour of radionuclides. Lower K_d values were observed for sandy and organic soils. Although K_d values quantitatively represent the soil water interaction and migration to some extent, the effect of elapsed time since the incorporation of the radionuclide where a fraction may become fixed by the solid phase (an aging effect related to sorption dynamics) in field studies could not be ignored. In real situations, vertical movement of Cs decreases with time. Though there are numerous data of Cs-K_d for different soil characteristics, limited data is available for vertical variability which has pronounced effect on Cs soil profile concentration. Therefore, data provided in the present study will be useful for explaining the shape of Cs soil profile on long term at the respective site.

5.3. Effect of soil parameters on migration

A few soil parameters show a strong effect on vertical migration. Since our sample size is small, at this stage it is not easy to understand the mechanism of the physical process for migration, which requires analyses of more soil cores in the particular area in the future.

5.4. Analytical profiles

Fitting analytical profiles was moderately successful. Given that the profiles were essentially falling exponential in shape, or linear in log scale, models which imply concave (downwards bent) functions in log scale, such as Gaussian type ones, had to be discarded, and only ones which are asymptotically (for deeper layers) exponential were retained. These are, at current stage, the CDE1, CDEfix and SimpSorp models. The first and the third provided numerically reasonable results; which is not to say that they are physically correct.

Validating the results and possibly deciding about the adequacy of a model requires soil profiles with higher resolution in the topmost few cm, say down to 4 or 5 cm. If practically achievable, fine resolution with layers < 1 cm thick should be achieved. The feasibility has to be evaluated in a future sampling campaign in the region, possibly trying different sampling techniques.

5.5. Compartment models

The compartment model could be applied to all except one profile (FL-2B). Typical migration velocities derived with this method are between 0.7 and 2.5 cm y^{-1}. It seems that migration is somewhat slower in grassland than in forest soils, but further samples would be needed for statistical validation.

5.6. Synthesis: transport rates

The most robust, and easiest to calculate transport rates, expressed as velocities, are the empirical ones (2.5.1), followed by the ones corresponding the compartment model (Section 2.8) and the empirical or descriptive models (exponential and “expon-alpha”, Section 2.7.1). However they serve different purposes and so do, in consequence, the derived migration parameters. In any case, migration of Cs in the investigated soils is slow, with bulk velocities (see Section 4.1; derived from empirical profiles or as means over models) in the order 1 cm y^{-1}, and velocities resulting from fitted physical models, if feasible at all, fractions of 1 cm y^{-1}.

The findings may be compared with previous knowledge. An overview on migration parameters is given in IAEA (2009, 2010). Migration velocities of Cs are mostly in the order of a few mm/y, with higher rates in organic soils. Bulk velocities found in our study are higher than these, whereas velocities inferred from physical models (v* of SimpSorp in particular Table 9) are in the same order, mm y^{-1}. Bossew and Kirchner (2004), after investigating several hundred soil profiles taken all over Austria few years after the Chernobyl accident, found differences in migration velocities with higher values in lowland than in upland soils.

Migration velocity was positively correlated with organic matter content, and negatively with the content of silicate minerals.

In a number of post-Fukushima studies carried out in the contaminated region, generally lower bulk migration velocities were found than in our study (Section 4.4).

5.7. Outlook: Suggestions for further studies

The small-scale local variability of inventories (samples A and B for four locations) appeared very high. This phenomenon should be validated by taking a larger number of samples (suggested 10 to 20) within a small neighbourhood of a few meters size, possibly following the scheme in Lettner et al. (2000).

As suggested earlier, profiles with finer resolution, i.e. less thick soil layers should be taken. This is especially important within the first few cm, where the concentration gradients can be expected most pronounced. For fitting analytical profiles for the sake of estimating physical migration parameters, sampling this very part of the profile is essential for reliable parameter estimates.

Possible sampling effects should be investigated more deeply. The procedure of sampling soil cores involves a number of sources of error and uncertainty, caused by deformation of the soil, cross-contamination of layers, ill-treatment of the litter layer for forest soil, etc. It is suggested to perform a series of experiments to optimize the procedure and to check repeatability and reproducibility.

Finally, it would be worthwhile to compare migration rates of Cs with ones of other radionuclides. Candidates among long-lived ones are ^{90}Sr and Pu isotopes. However these were released by the FNPP accident only to a very small extent, hence their concentrations in soil are very low, which renders the analytical effort more difficult, than for ^{137}Cs.

Acknowledgements

This research was supported by a Grant-in-Aid for Scientific Research from the Japan Society for the Promotion of Science (11P11503). SM is thankful to the Japan Society for the Promotion of Science for the award of post-doctoral fellowship.

Appendix Annex A. Measurement results

Measurement results for depth profile parameters (bulk density, porosity, Cs activity concentration (both gravimetric, C_m (Bq kg^{-1}) and volumetric, C_v (Bq L^{-1})), residence time (τ) and migration velocity (v) derived from the compartmental model for each layer in 10 soil cores collected from six sites).

Sample No.	Sampling date M/D/Y	Soil depth cm	Reference soil depth cm	Mass depth middle point g cm^{-2}	Bulk density kg L^{-1}	Porosity %	Distribution coefficient L kg^{-1}
GL-1(A)	11/8/2012	0–2	1.0	1.31	1.31	50.63	426.96
		2–4	3.0	2.97	0.99	62.54	367.8
		4–6	5.0	6.55	1.31	50.44	367.8
		6–8	7.0	9.59	1.37	48.13	482.6
		8–10	9.0	9.99	1.11	58.02	356.6
		10–15	12.5	17.00	1.36	48.82	399.8
		15–20	17.5	17.50	1.00	70.95	405.6
GL-1(B)	9/26/2012	0–2	1.0	1.31	1.31	50.70	388.0
		2–4	3.0	4.14	1.38	47.96	453.0
		4–6	5.0	7.85	1.57	40.71	467.0
		6–8	7.0	9.10	1.30	50.93	387.0
		8–10	9.0	9.45	1.05	60.56	400.0
		10–15	12.5	17.75	1.42	46.49	462.0
GL-2(A)	11/7/2012	0–2	1.0	2.09	2.09	21.14	77.0
		2–4	3.0	5.55	1.85	30.17	86.0
		4–6	5.0	7.50	1.50	43.42	76.0
		6–8	7.0	9.66	1.38	48.03	83.0
		8–10	9.0	8.73	0.97	63.50	75.0
GL-2(B)	6/27/2013	0–5	2.5	3.15	1.26	52.39	220.3
		5–10	7.5	7.95	1.06	59.85	266.1
		10–15	12.5	10.37	0.83	68.79	230.2
GL-3	6/28/2013	0–5	2.5	2.47	0.99	62.77	47.15
		5–10	7.5	8.10	1.08	59.10	64.7
		10–15	12.5	11.25	0.90	65.95	67.56
		15–20	17.5	21.00	1.20	54.80	53.71
FL-1(A)	11/8/2012	0–2	1.0	1.03	1.03	61.10	128.0
		2–4	3.0	3.42	1.14	57.06	167.0
		4–6	5.0	5.30	1.06	59.85	156.0
		6–8	7.0	7.77	1.11	58.22	148.0
		8–10	9.0	8.91	0.99	69.84	120.0
		10–15	12.5	10.12	0.81	74.68	123.0
		15–20	17.5	14.35	0.82	81.06	114.0
FL-1(B)	9/26/2012	0–2	1.0	0.65	0.65	75.59	111.0
		2–4	3.0	2.61	0.87	67.18	120.0
		4–6	5.0	3.45	0.69	74.07	123.0
		6–8	7.0	5.88	0.84	68.36	143.0
		8–13	10.5	10.29	0.98	62.90	127.0
FL-2(A)	11/8/2012	0–2	1.0	1.23	1.23	53.51	234.0
		2–4	3.0	3.00	1.00	62.35	218.0
		4–6	5.0	7.20	1.44	45.63	210.0
		6–8	7.0	7.07	1.01	61.96	246.0
		8–10	9.0	8.91	0.99	62.73	225.8
		10–15	12.5	12.12	0.97	63.27	220.3
		15–20	17.5	16.45	0.94	64.54	211.5
FL-2(B)	6/28/2013	0–5	2.5	2.03	0.81	69.26	173.9
		5–10	7.5	5.55	0.74	71.96	225.8
		10–15	12.5	8.75	0.70	73.56	220.3
		15–20	17.5	18.02	1.03	61.27	211.5
FL-3	6/28/2013	0–5	2.5	1.15	0.46	82.75	107.6
		5–10	7.5	3.30	0.44	83.35	54.0
		10–15	12.5	8.62	0.69	74.07	56.4
		15–20	17.5	12.07	0.69	74.02	55.8

Appendix Annex B. Correlation between soil parameters and major oxides Pearson correlation coefficient with significance among various soil parameters

Sample No.	Retardation factor R_d	Cs activity kBq kg^{-1}	Cs activity Bq cm^{-3}	$^{137}Cs/^{134}Cs$ ratio	τ y	V cm y^{-1}		
		^{137}Cs	^{134}Cs	^{137}Cs	^{134}Cs			
GL-1(A)	1105.7	47.9 ± 0.10	47.1 ± 0.18	62.8 ± 0.11	61.7 ± 0.11	1.02	1.91	1.05
	583.2	30.2 ± 0.10	29.0 ± 0.18	35.1 ± 0.03	28.7 ± 0.02	1.04	1.90	1.05
	956.2	5.21 ± 0.04	5.44 ± 0.05	6.82 ± 0.03	7.12 ± 0.02	0.96	1.90	1.05
	1374.7	4.66 ± 0.04	4.55 ± 0.05	4.38 ± 0.02	6.23 ± 0.02	1.02	1.90	1.05
	683.2	0.82 ± 0.02	0.72 ± 0.02	0.91 ± 0.02	0.80 ± 0.01	1.14	1.90	1.05
	1114.7	1.52 ± 0.02	1.45 ± 0.04	2.07 ± 0.08	1.97 ± 0.08	1.05	1.90	2.63
	572.7	1.64 ± 0.08	1.52 ± 0.11	1.64 ± 0.08	1.52 ± 0.06	1.07	1.90	2.63
GL-1(B)	1003.5	58.4 ± 0.10	57.6 ± 0.19	76.6 ± 0.08	75.5 ± 0.05	1.01	1.03	1.94
	1304.5	45.9 ± 0.10	44.6 ± 0.19	63.4 ± 0.07	61.5 ± 0.04	1.03	1.03	1.94
	1802.0	27.1 ± 0.10	26.0 ± 0.19	42.6 ± 0.08	40.8 ± 0.06	1.04	1.03	1.94
	988.8	16.7 ± 0.10	16.7 ± 0.19	21.7 ± 0.10	21.7 ± 0.09	1.00	1.03	1.94
	694.5	7.30 ± 0.10	7.43 ± 0.07	7.67 ± 0.08	7.80 ± 0.05	0.98	1.03	1.94
	1412.1	2.98 ± 0.11	3.30 ± 0.25	4.24 ± 0.02	4.68 ± 0.01	0.91	1.03	4.86
GL-2(A)	762.3	6.44 ± 0.04	6.59 ± 0.05	13.5 ± 0.02	13.8 ± 0.01	0.98	2.32	0.86
	528.3	5.10 ± 0.04	5.08 ± 0.05	9.44 ± 0.00	9.39 ± 0.01	1.01	2.30	0.87
	263.6	0.08 ± 0.01	0.09 ± 0.01	0.12 ± 0.00	0.13 ± 0.00	0.92	2.30	0.87
	239.5	0.03 ± 0.00	0.04 ± 0.01	0.04 ± 0.01	0.05 ± 0.01	0.86	2.30	0.87
	115.6	0.03 ± 0.01	0.03 ± 0.01	0.03 ± 0.04	0.03 ± 0.03	0.95	2.30	0.87
GL-2(B)	530.8	12.6 ± 0.05	12.6 ± 0.07	15.1 ± 0.06	15.8 ± 0.06	1.00	6.93	0.72
	472.3	3.58 ± 0.03	3.63 ± 0.04	3.80 ± 0.03	3.84 ± 0.03	0.99	6.83	0.73
	278.8	1.35 ± 0.02	1.43 ± 0.02	1.12 ± 0.01	1.19 ± 0.01	0.95	6.83	0.73
GL-3	75.4	68.1 ± 0.12	68.9 ± 0.17	67.5 ± 0.12	68.2 ± 0.12	0.99	7.89	0.63
	119.2	16.1 ± 0.05	16.2 ± 0.08	17.4 ± 0.05	17.5 ± 0.05	1.00	7.70	0.65
	93.2	1.80 ± 0.03	1.79 ± 0.05	1.62 ± 0.04	1.61 ± 0.04	1.00	7.70	0.65
	118.6	0.53 ± 0.03	0.53 ± 0.04	0.64 ± 0.02	0.63 ± 0.02	1.01	7.70	0.65
FL-1(A)	216.8	138.9 ± 0.21	144.2 ± 0.37	143.1 ± 0.20	148.5 ± 0.2	0.96	1.18	1.69
	334.6	66.7 ± 0.21	68.9 ± 0.18	76.2 ± 0.18	78.5 ± 0.16	0.97	1.18	1.70
	277.3	54.7 ± 0.08	56.8 ± 0.13	58.0 ± 0.08	60.2 ± 0.08	0.96	1.18	1.70
	283.2	39.6 ± 0.1	41.9 ± 0.18	44.0 ± 0.09	46.5 ± 0.08	0.95	1.18	1.70
	171.1	14.6 ± 0.1	14.7 ± 0.18	14.4 ± 1.11	14.4 ± 0.11	1.00	1.18	1.70
	134.4	20.8 ± 0.1	21.9 ± 0.18	16.9 ± 0.13	17.7 ± 0.16	0.95	1.18	4.24
	116.3	7.00 ± 0.1	7.41 ± 0.18	5.74 ± 1.45	6.08 ± 0.22	0.94	1.18	4.24
FL-1(B)	96.4	1303 ± 0.94	1343 ± 1.31	846.8 ± 0.24	873.1 ± 0.28	0.97	3.01	0.67
	156.4	113.8 ± 0.21	117.7 ± 0.37	99.0 ± 0.30	102.4 ± 0.44	0.97	3.01	0.67
	115.6	63.7 ± 0.21	65.4 ± 0.19	43.9 ± 0.25	45.1 ± 0.30	0.97	3.01	0.67
	176.7	106.5 ± 0.21	108.0 ± 0.37	89.4 ± 0.11	90.7 ± 0.11	0.99	3.01	0.67
	198.9	68.9 ± 0.10	70.7 ± 0.19	67.5 ± 0.08	69.3 ± 0.06	0.97	3.01	1.66
FL-2(A)	538.9	756.3 ± 0.52	798.3 ± 0.18	930.3 ± 0.10	982.0 ± 0.10	0.95	14.59	0.14
	350.6	41.7 ± 0.10	43.6 ± 0.18	41.7 ± 0.07	43.6 ± 0.05	0.96	3.01	0.66
	663.7	40.6 ± 0.10	41.6 ± 0.18	58.5 ± 0.10	60.0 ± 0.10	0.98	3.01	0.66
	402.0	13.5 ± 0.10	14.5 ± 0.18	13.7 ± 0.02	14.6 ± 0.02	0.93	3.01	0.66
	357.4	0.73 ± 0.02	0.72 ± 0.02	0.72 ± 0.11	0.72 ± 0.11	1.01	3.01	0.66
	338.7	0.26 ± 0.10	0.27 ± 0.18	0.25 ± 0.11	0.26 ± 0.12	0.96	3.01	1.66
	309.0	0.15 ± 0.10	0.15 ± 0.09	0.14 ± 0.18	0.14 ± 0.22	1.00	3.01	1.66
FL-2(B)	204.4	97.0 ± 0.15	98.8 ± 0.22	78.8 ± 0.04	80.0 ± 0.05	0.98	NA	NA
	233.2	3.33 ± 0.03	3.32 ± 0.04	2.46 ± 0.03	2.46 ± 0.04	1.00	NA	NA
	210.6	1.54 ± 0.02	1.52 ± 0.03	1.08 ± 0.01	1.06 ± 0.01	1.01	NA	NA
	356.5	0.40 ± 0.01	0.38 ± 0.01	0.41 ± 0.22	0.39 ± 0.48	1.05	NA	NA
FL-3	60.8	31.1 ± 0.10	31.4 ± 0.15	14.3 ± 0.18	14.5 ± 0.41	0.99	1.95	2.56
	29.5	18.7 ± 0.08	18.8 ± 0.11	8.23 ± 0.07	8.28 ± 0.10	0.99	1.95	2.56
	53.5	8.06 ± 0.05	8.24 ± 0.01	5.56 ± 0.07	5.69 ± 0.10	0.98	1.96	2.56
	53.0	8.62 ± 0.05	8.82 ± 0.07	5.95 ± 0.03	6.08 ± 0.03	0.98	1.96	2.56

τ = residence time (y), V = migration velocity (cm y^{-1}) derived from compartmental model.

		pH	OC	$CaCO_3$	Ex. Ca	Ex. K	Ex. Mg	Ex. Na	CEC_b	Sand	Silt + clay	K_d	SiO_2	TiO_2
pH	Pearson Corr.	1												
	Sig.	–												
OC	Pearson Corr.	−0.71	1.00											
	Sig.	0.12	–											
$CaCO_3$	Pearson Corr.	0.56	−0.22	1.00										
	Sig.	0.25	0.68	–										
Ex. Ca	Pearson Corr.	**0.82**	−0.32	0.79	1.00									
	Sig.	**0.05**	0.53	0.06	–									
Ex. K	Pearson Corr.	−0.13	0.14	−0.14	−0.03	1.00								
	Sig.	0.80	0.79	0.79	0.95	–								
Ex. Mg	Pearson Corr.	−0.52	0.57	−0.12	−0.22	**0.86**	1.00							
	Sig.	0.29	0.24	0.82	0.68	**0.03**	–							
Ex. Na	Pearson Corr.	−0.76	0.66	−0.19	−0.31	0.05	0.45	1.00						
	Sig.	0.08	0.15	0.72	0.56	0.93	0.37	–						
CECb	Pearson Corr.	0.72	−0.21	0.77	**0.97**	0.18	0.02	−0.22	1.00					
	Sig.	0.11	0.69	0.07	**0.00**	0.73	0.98	0.68	–					
Sand	Pearson Corr.	−0.09	−0.20	−0.10	−0.47	−0.61	−0.53	−0.35	−0.61	1.00				
	Sig.	0.86	0.71	0.85	0.35	0.19	0.27	0.49	0.20	–				
Silt + clay	Pearson Corr.	0.09	0.15	0.13	0.45	0.72	0.62	0.30	0.61	**−0.99**	1.00			
	Sig.	0.86	0.78	0.81	0.38	0.11	0.19	0.56	0.20	**0.00**	–			
K_d	Pearson Corr.	−0.14	0.18	−0.28	−0.05	**0.98**	**0.81**	0.06	0.15	−0.67	0.75	1.00		
	Sig.	0.80	0.74	0.59	0.92	**0.00**	**0.05**	0.91	0.78	0.15	0.09	–		
SiO_2	Pearson Corr.	0.64	**−0.98**	0.22	0.31	−0.28	−0.64	−0.52	0.17	0.21	−0.18	−0.31	1.00	
	Sig.	0.17	**0.00**	0.67	0.55	0.60	0.17	0.29	0.74	0.69	0.73	0.55	–	
TiO_2	Pearson Corr.	−0.12	−0.19	0.12	0.05	0.70	0.61	0.29	0.21	−0.54	0.64	0.60	0.18	1.00
	Sig.	0.82	0.72	0.83	0.92	0.12	0.20	0.58	0.70	0.27	0.17	0.20	0.73	–
Al_2O_3	Pearson Corr.	−0.11	0.06	−0.44	−0.42	−0.74	−0.66	−0.18	−0.59	0.71	**−0.80**	−0.64	−0.01	**−0.88**
	Sig.	0.83	0.91	0.38	0.41	0.09	0.15	0.74	0.22	0.12	**0.05**	0.17	0.98	**0.02**
Fe_2O_3	Pearson Corr.	−0.19	0.07	−0.10	−0.09	**0.97**	**0.86**	0.10	0.12	−0.53	0.66	**0.91**	−0.19	**0.81**
	Sig.	0.71	0.89	0.86	0.86	**0.00**	**0.03**	0.85	0.82	0.28	0.15	**0.01**	0.72	**0.05**
MgO	Pearson Corr.	0.54	0.07	0.29	0.57	0.44	0.23	−0.50	0.64	−0.41	0.43	0.47	−0.24	−0.13
	Sig.	0.27	0.90	0.58	0.24	0.39	0.67	0.31	0.17	0.42	0.39	0.35	0.65	0.81
CaO	Pearson Corr.	0.57	0.06	0.53	0.56	−0.10	−0.16	−0.59	0.53	0.09	−0.09	−0.11	−0.17	−0.52
	Sig.	0.24	0.92	0.28	0.25	0.85	0.76	0.22	0.28	0.87	0.86	0.83	0.75	0.29
Na_2O	Pearson Corr.	0.63	**−0.84**	0.16	0.17	−0.58	**−0.87**	−0.71	−0.02	0.61	−0.60	−0.60	**0.85**	−0.32
	Sig.	0.18	**0.03**	0.76	0.75	0.22	**0.02**	0.12	0.96	0.20	0.20	0.21	**0.03**	0.54
K_2O	Pearson Corr.	0.68	**−0.86**	0.10	0.31	−0.54	**−0.88**	−0.56	0.12	0.30	−0.34	−0.50	**0.90**	−0.23
	Sig.	0.13	**0.03**	0.85	0.55	0.27	**0.02**	0.24	0.83	0.56	0.51	0.31	**0.01**	0.66
P_2O_5	Pearson Corr.	−0.37	0.51	0.35	−0.13	0.36	0.64	0.17	0.01	0.08	0.01	0.21	−0.58	0.20
	Sig.	0.47	0.30	0.50	0.81	0.49	0.17	0.75	0.98	0.88	0.98	0.69	0.23	0.71
MnO	Pearson Corr.	0.21	0.22	0.39	0.28	0.55	0.51	−0.38	0.41	−0.15	0.24	0.47	−0.40	0.06
	Sig.	0.70	0.67	0.45	0.59	0.26	0.30	0.46	0.43	0.77	0.64	0.35	0.43	0.91
v (EC)	Pearson Corr.	−0.79	**0.90**	−0.08	−0.45	0.06	0.55	0.64	−0.34	0.08	−0.09	0.02	**−0.87**	−0.10
	Sig.	0.06	**0.01**	0.88	0.37	0.91	0.26	0.17	0.51	0.88	0.87	0.98	**0.02**	0.85
t (CM)	Pearson Corr.	0.29	−0.54	−0.35	−0.30	−0.37	−0.64	−0.73	−0.45	0.73	−0.72	−0.33	0.48	−0.50
	Sig.	0.58	0.27	0.50	0.57	0.47	0.18	0.10	0.37	0.10	0.11	0.52	0.34	0.31
D (EC)	Pearson Corr.	**−0.81**	**0.90**	−0.12	−0.43	0.32	0.75	0.67	−0.28	−0.11	0.13	0.27	**−0.89**	0.13
	Sig.	**0.05**	**0.02**	0.82	0.39	0.54	0.08	0.15	0.59	0.83	0.80	0.60	**0.02**	0.81
V (CM)	Pearson Corr.	−0.66	0.61	0.00	−0.14	0.25	0.60	**0.96**	−0.01	−0.51	0.49	0.22	−0.49	0.49
	Sig.	0.16	0.20	0.99	0.80	0.64	0.20	**0.00**	0.99	0.30	0.32	0.67	0.32	0.32
ρ	Pearson Corr.	0.64	**−0.84**	0.48	0.57	−0.09	−0.39	−0.26	0.50	−0.18	0.21	−0.15	**0.88**	0.46
	Sig.	0.17	**0.04**	0.34	0.24	0.86	0.44	0.62	0.31	0.74	0.69	0.77	**0.02**	0.36
θ	Pearson Corr.	−0.72	**0.87**	−0.51	−0.62	0.11	0.44	0.36	−0.54	0.15	−0.18	0.17	**−0.90**	−0.38
	Sig.	0.11	**0.03**	0.30	0.19	0.83	0.38	0.49	0.27	0.78	0.74	0.75	**0.02**	0.45

	Al_2O_3	Fe_2O_3	MgO	CaO	Na_2O	K_2O	P_2O_5	MnO	V (EC)	t (CM)	D (EC)	V (CM)	ρ	θ
pH														
OC														
$CaCO_3$														
Ex. Ca														
Ex. K														
Ex. Mg														
Ex. Na														
CECb														
Sand														
Silt + clay														
K_d														
SiO_2														
TiO_2														
Al_2O_3	1.00													
	–													
Fe_2O_3	− 0.79	1.00												
	0.06	–												
MgO	− 0.27	0.27	1.00											
	0.60	0.60	–											
CaO	0.09	− 0.22	**0.80**	1.00										
	0.86	0.67	**0.06**	–										
Na_2O	0.43	− 0.53	− 0.17	0.13	1.00									
	0.39	0.28	0.74	0.80	–									
K_2O	0.35	− 0.53	− 0.16	− 0.01	**0.92**	1.00								
	0.50	0.28	0.76	0.99	**0.01**	–								
P_2O_5	− 0.37	0.42	0.18	0.29	− 0.50	− 0.77	1.00							
	0.47	0.41	0.74	0.58	0.31	0.07	–							
MnO	− 0.41	0.48	0.79	0.72	− 0.31	− 0.50	0.71	1.00						
	0.42	0.34	0.06	0.11	0.55	0.31	0.11	–						
v (EC)	0.04	0.08	− 0.15	− 0.01	− 0.72	**− 0.86**	0.73	0.24	1.00					
	0.94	0.88	0.77	0.99	0.11	**0.03**	0.10	0.65	–					
t (CM)	0.68	− 0.38	− 0.07	0.13	0.78	0.63	− 0.40	− 0.16	− 0.48	1.00				
	0.14	0.46	0.89	0.81	0.07	0.18	0.44	0.76	0.34	–				
D (EC)	− 0.18	0.33	− 0.07	− 0.09	**− 0.85**	**− 0.96**	0.77	0.33	**0.96**	− 0.58	1.00			
	0.73	0.52	0.89	0.87	**0.03**	**0.00**	0.08	0.53	**0.00**	0.22	–			
V (CM)	− 0.45	0.31	− 0.36	− 0.52	− 0.78	− 0.64	0.31	− 0.18	0.61	**− 0.88**	0.69	1.00		
	0.37	0.55	0.49	0.29	0.07	0.17	0.55	0.73	0.20	**0.02**	0.13	–		
ρ	− 0.40	0.00	− 0.14	− 0.19	0.56	0.69	− 0.44	− 0.30	− 0.76	0.02	− 0.72	− 0.14	1.00	
	0.43	1.00	0.79	0.73	0.25	0.13	0.39	0.56	0.08	0.98	0.10	0.79	–	
θ	0.36	0.04	0.06	0.08	− 0.61	− 0.73	0.44	0.25	**0.80**	− 0.08	0.77	0.23	− 0.99	1.00
	0.48	0.95	0.91	0.87	0.20	0.10	0.38	0.64	**0.05**	0.89	0.07	0.65	0.00	—>

V: migration velocity, D: diffusion coefficient, t: residence time, EC: empirical calculation, CM: compartmental model, ρ: bulk density, θ: porosity. Significant correlations (prob(H0: r = 0) ≤ 0.05) printed bold.

Appendix Annex C. : The fitting algorithm

C.1. The algorithm

The chosen fitting algorithm is a relatively crude one, made such as to avoid the chance, as well as possible with easy computational means, being trapped in local minima of the loss function. Better ones may be used in the future. For complicated functions such as CDE1 algorithms implemented in common software tend not to perform very well, however.

The loss function is defined as $\varphi(a_1,\ldots,a_m) = (1/n)\ \Sigma_{i\ =\ 1\ldots n}\ [\log(f_i(a_1,\ldots,a_m)) - \log(C_i)]^2$, f_i – the model and C_i the data at observation (no. of layer) i of the profile. The log-transform has been chosen to honour small values alike high ones. No statistical goodness of fit tests were performed at this stage.

Starting from guessed start values of the parameters to be estimated, $a_1,\ldots,a_m$, (the choice is not very sensitive), a hypercube with side length da_1, $\ldots,da_m$ centred around the a_i is built and random values of $a_1,\ldots,a_m$ chosen within. φ is computed and if it is smaller than the previous one, the new set of parameters {a} is adopted, and so on. At each successful reduction of φ, the size of the cube, centred around the new values, is reduced (5% reduction chosen). (A Latin hypercube design may be more efficient, e.g. Wyss and Jorgensen (1998). Also "escapes" such as in simulated annealing may be useful.)

The integral z = 0 to ∞, which is normally treated as free parameter, is fixed to the observed inventory here, which is a reliable quantity. The profile "tail" is negligible in most cases, since the bulk activity resides in higher layers. Ignoring the tail part is therefore no great error.

The migration time is the one between 15 March 2011 and the sampling date.

The loop is terminated after either 50,000 iterations or if $|1 - \varphi/\varphi(\text{previous})| < 1e-8$. The algorithm is not elegant but appears robust. Computation time is a few seconds, at most. It has been programmed in QBasic using QB64 compiler which is usually quite fast.

Fitting the CDE profile including a fixed phase ("CDEfix") is slower because an additional temporal numerical integration step is required. (The simple trapezoid method has been used, time step 0.02 years starting at t = 0.02. t = 0 would result in division by zero. The total loop has been restricted to 20,000 iterations here.)

In the programs, erfc and Bessel functions have to be implemented. For erfc, an approximation given by Winitzki (2008) with α parameter 0.147 (see also Soranzo and Epure, 2012) was used. For the Bessel functions I_0 and I_1 we used the formulas 9.8.1 ff. (p.378) from (Abramowitz and Stegun, 1972).

C.2. The CDE1 model

For bad fits – which holds for the profiles investigated here except the CDE1 model for GL-1B – the danger of the algorithm being trapped in local minima of φ is probably still present. The CDE1 fitting results of 10 runs for profile GL-1B are shown in Table C1, showing slightly different solutions

Table C1
CDE1 fitting parameters, profile GL-1B, for 10 test runs of the algorithm.

Run code	v cm y^{-1}	D cm^2 y^{-1}	m cm^{-1}	φ
01	0.280	0.867	0.313	0.02744347
02	0.284	0.842	0.313	0.02744172
03	0.281	0.875	0.314	0.02744485
04	0.288	0.841	0.313	0.02744364
05	0.285	0.836	0.313	0.02744181
06	0.280	0.856	0.313	0.02744410
07	0.287	0.821	0.312	0.02744465
08	0.282	0.856	0.313	0.02744586
09	0.288	0.838	0.314	0.02744308
10	0.276	0.891	0.313	0.02744501

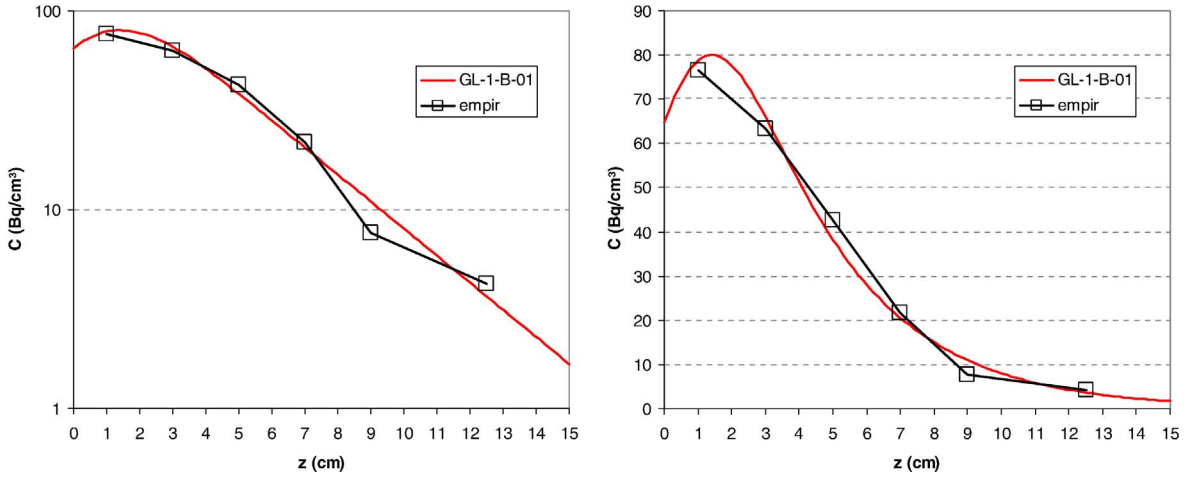

Fig. C1. The CDE1 fitted profile GL-1B together with the empirical profile in linear and logarithmic scale. The parameters are given in Table C1.

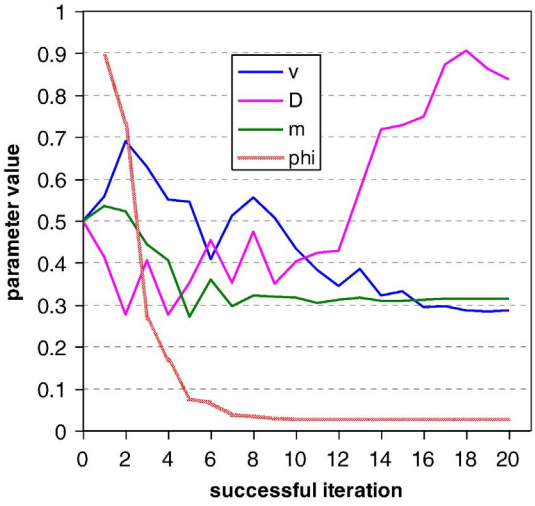

Fig. C2. Traces of the parameter values, profile GL-2B, test run 09 of CDE1 fit (see Table C1). Initial guesses: v = 0.5 cm y^{-1}, D = 0.5 cm^2 y^{-1} and m = 0.5 cm^{-1}.

corresponding to very similar minimal φ at which the algorithm has stopped. A slow rate of reduction of the cubes can to some extent reduce the chance of such trap but also slows the algorithm. Fig. C1 shows the CDE1 fitted profile and the empirical profile; differences between the 10 solutions, Table C1, are not visible in the graph. The example has been chosen for demonstration because the characteristic CDE1 shape is best developed for this profile.

Fig. C2 shows the traces of the parameter estimates with successful iterations (i.e. the ones which result in reduced φ). One can recognize that stable values of v and m are attained relatively quickly whereas the dispersion D fluctuates more strongly without really converging. One may think on improving the algorithm by requiring a convergence condition for all parameters individually, not only the φ as implemented here, but this would increase computation time.

Table C1: CDE1 fitting parameters, profile GL-1B, for 10 test runs of the algorithm.

The variability between the results may be considered as the uncertainty of the results. In this case the AM (CV) of v, D and m are 0.283 cm y^{-1} (1.4%), 0.853 cm^2 y^{-1} (2.5%) and 0.313 cm^{-1} (0.2%), respectively. Other profile fittings are less instructive since they consist of the exponential component only, see Table C1.

C.3. The CDEfix model

In Table C2 ten runs for fitting the CDEfix model are presented. The results depend strongly on the initial guess of the parameter "f" which is not satisfying. The solutions correspond to relatively high RSS values φ, compared to the ones shown for the CDE1 fit, Table C1. Fig. C3 shows that the model is certainly not adequate which renders the inconsistent fitting results unsurprising. Also the values of the fixation rate seem too low compared to what the experimental results about the F5 fraction suggest.

Table C2
CDE fix fitting parameters, profile GL-1B, for 10 test runs of the algorithm.

Run code	Initial guess of f	v cm y^{-1}	D cm^2 y^{-1}	f y^{-1}	φ
01	0.05	0.71	2.92	0.020	2.83
02	0.2	1.59	3.05	0.18	1.06
03	0.5	1.62	3.03	0.002	0.905
04	0.5	1.91	2.79	0.012	0.908
05	0.8	1.01	3.11	< 0.001	1.62
06	0.2	1.45	2.74	0.099	1.75
07	0.05	0.64	3.18	< 0.001	2.23
08	0.1	0.78	2.80	0.002	3.06
09	0.6	0.66	3.33	0.18	2.23
10	0.7	0.57	2.79	0.001	3.81

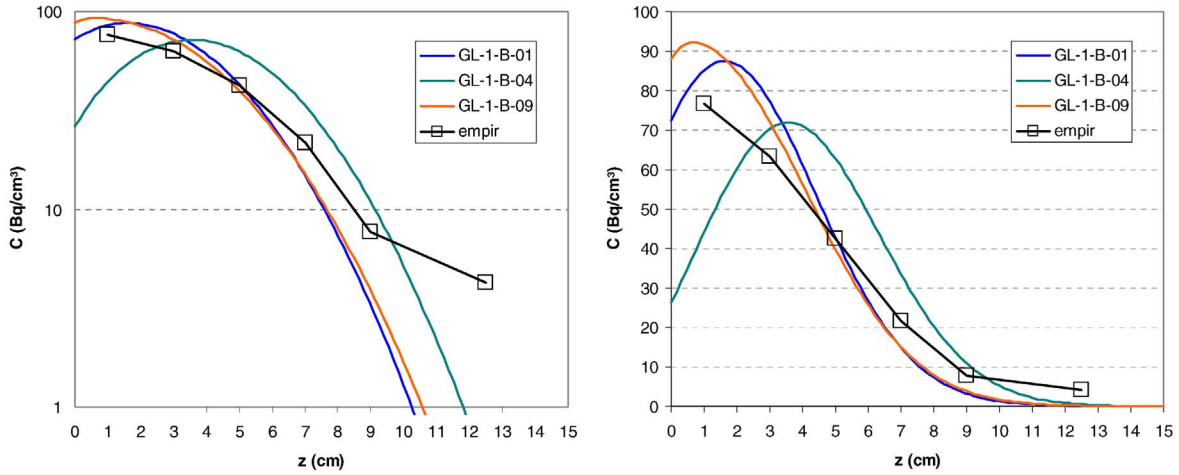

Fig. C3. The CDE fix fitted profile GL-1B together with the empirical profile in linear and logarithmic scale. The parameters are given in Table C2.

C.4. The SimpSorp model

Table C3 presents ten fitting runs of the SimpSorp model. The results of sorption parameters p_1 and p_2 vary relatively strongly, but remarkably the asymptotic velocities v* and dispersions D* do very little, in comparison, see the last line which shows the CVs over run results. These two parameters are the characteristic ones for describing the transport. No consistent dependence on the starting values can be recognized. Convergence is relatively slow, so that 100,000 iterations were chosen; even more could make sense. Computation time is low. Fig. C4 shows three fitted profiles. Visually no distinction is possible.

Table C3
SimpSorp fitting parameters, profile GL-1B, for 10 test runs of the algorithm.

Run code	v(0) cm d^{-1}	$p_1(0)$ d^{-1}	$p_2(0)$ d^{-1}	v cm d^{-1}	p_1 d^{-1}	$p_2(\times 10^{-3})$ d^{-1}	v* cm y^{-1}	D* cm^2 y^{-1}	− φ
1	0.5	0.5	0.02	1.790	0.926	1.67	1.182	2.287	0.03666633
2	0.8	0.3	0.01	1.134	0.675	1.66	1.178	2.293	0.03669215
3	0.6	0.7	0.02	1.308	0.676	1.69	1.196	2.314	0.03671956
4	0.7	0.7	0.003	1.045	0.535	1.65	1.179	2.303	0.03672225
5	1	0.4	0.003	1.472	0.760	1.68	1.187	2.3	0.03668307
6	1	0.6	0.002	1.530	0.788	1.66	1.178	2.285	0.03668273
7	1.2	0.5	0.003	1.863	0.960	1.67	1.182	2.295	0.03669464
8	1.2	0.5	0.003	1.543	0.793	1.67	1.182	2.298	0.03668114
9	0.7	0.4	0.005	1.762	0.913	1.69	1.189	2.295	0.03666599
10	0.7	0.4	0.005	2.209	1.144	1.69	1.188	2.293	0.03665041
AM				1.566	0.817	1.673	1.184	2.296	
CV (%)				23	21	0.85	0.49	0.36	

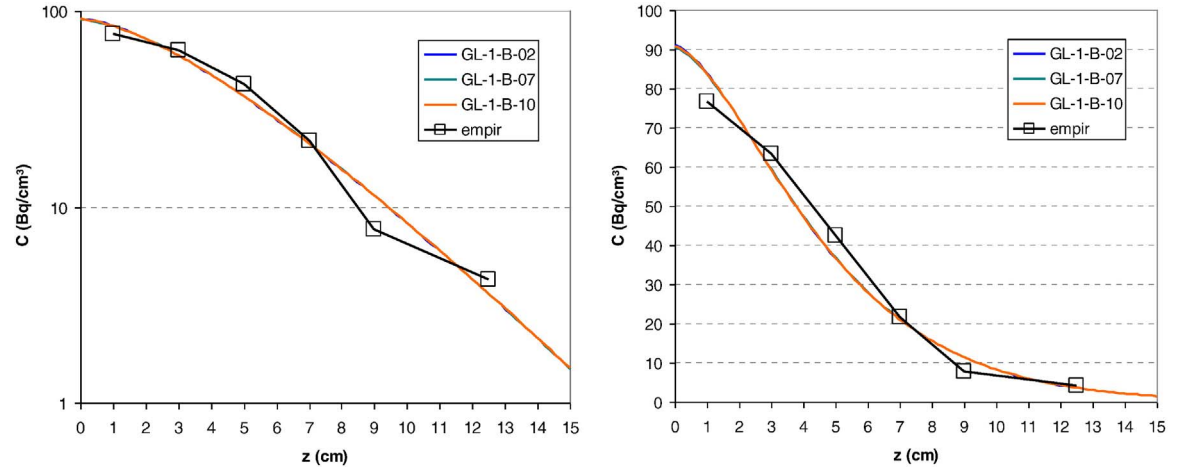

Fig. C4. The SimpSorp fitted profile GL-1B together with the empirical profile in linear and logarithmic scale. The parameters are given in Table C3.

References

Abramowitz, M. and Stegun, I.A. (Eds. Dec. 1972) [1964]. Handbook of Mathematical Functions With Formulas, Graphs, and Mathematical Tables, New York: Dover Publications, (ISBN 978-0-486-61272-0. In: http://www.cs.bham.ac.uk/~aps/research/projects/as/book.php (accessed 21 Nov 2015)).

Ajayi, I.R., 2010. Residence half-times of ^{137}Cs in undisturbed surface soil in Nigeria based on measured soil concentration profiles. Mod. Appl. Sci. 4, 31–40. http://dx.doi.org/10.5539/mas.v4n2p31.

Akaike, H., 1974. A new look at the statistical model identification. IEEE Trans. Autom. Control 19, 716–723. http://dx.doi.org/10.1109/tac.1974.1100705.(www.unt.edu/rss/class/Jon/MiscDocs/Akaike_1974.pdf).

Boone, F.W., Kantelo, M.V., Mayer, P.G., Palms, J.M., 1985. Residence half-times of ^{129}I in undisturbed surface soils based on measured soil concentration profiles. Health Phys. 48, 401–413. http://dx.doi.org/10.1097/00004032- 198504000-00002.

Bossew, P., Kirchner, G., 2004. Modelling the vertical distribution of radionuclides in soil. Part 1: the convection-dispersion equation revisited. J. Environ. Radioact. 73, 127–150. http://dx.doi.org/10.1016/j.jenvrad. 2003.08.006.

Bossew, P., Ditto, M., Falkner, T., Henrich, E., Kienzl, K., Rappelsberger, U., 2001. Contamination of Austrian soil with ^{137}Cs. J. Environ. Radioact. 55, 187–194. http://dx.doi.org/10.1016/s0265-931x(00)00192-2.

Bossew, P., Gastberger, M., Gohla, H., Hofer, P., Hubmer, A., 2004. Vertical distribution of radionuclides in soil of a grassland site in Chernobyl exclusion zone. J. Environ. Radioact. 73, 87–99. http://dx.doi.org/10.1016/j. jenvrad. 2003.08.004.

Bunzl, K., 2001. Migration of fallout-radionuclides in the soil: effects of non-uniformity of the sorption properties on the activity-depth profiles. Radiat. Environ. Biophys. 40, 237–241.

Bunzl, K., 2002. Vertical random variability of the distribution coefficient in the soil and its effect on the migration of fallout radionuclides. J. Radioanal. Nucl. Chem. 254, 15–21.

Bunzl, K., Förster, H., Kracke, W., Schimmack, W., 1994. Residence times of fallout $^{239+240}$Pu, ^{238}Pu, ^{241}Am and ^{137}Cs in the upper horizons of an undisturbed grassland soil. J. Environ. Radioact. 22, 11–27.

Burnham, K.P., Anderson, D.R., 2004. Multimodel inference: understanding AIC and BIC in model selection. Sociol. Methods Res. 33, 261–304.

Coleman, N.T., Craig, D., Lewis, R.J., 1963. Ion-exchange reactions of cesium. Soil Sci. Soc. Am. J. 27, 287–289.

Cornell, R.M., 1993. Adsorption of cesium on minerals: a review. J. Radioanal. Nucl. Chem. 171, 483–500. http://dx.doi.org/10.1007/ bf02219872.

Denk, H.J., Felsmann, M., 1989. Measurement and evaluation of a compartment model for estimating future activity profiles of radiocaesium in undisturbed soil of pasture-land in North Rhine-Westfalia. In: Feldt, W. (Ed.), Radioecology of Natural and Artificial Radionuclides, Proceedings of the XVth Regional Congress of IRPA, Visby, Sweden, 10–14 Sept. TUV Rheinland, Koln, Ber. FS-48-T, pp. 182–187.

Devell, L., 1991. Composition and properties of plume and fallout materials from the Chernobyl accident. In: Moberg, L. (Ed.), The Chernobyl Fallout in Sweden. SSI, Stockholm, pp. 29–46.

Drissner, J., Bürmann, W., Enslin, F., Heider, R., Klemt, E., Miller, R., Schick, G., Zibold, G., 1998. Availability of caesium radionuclides to plant-classification of soils and role of mycorrhiza. J. Environ. Radioact. 41, 19–32. http://dx.doi.org/10.1016/S0265-931X(97)00092-1.

Erlandsson, B., Asking, L., Swietlicki, E., 1987. Detailed early measurements of the fallout in Sweden from Chernobyl accident. Water Air Soil Pollut. 35, 335–347.

Evans, E.J., Dekker, A.J., 1967. The effect of soil organic matter content on the ^{137}Cs concentration in crops. Can. J. Soil Sci. 47, 7–13.

Francis, C.W., Brinkley, F.S., 1976. Preferential adsorption of ^{137}Cs to micaceous minerals in contaminated freshwater sediment. Nature 260, 511–513 (C:\Users\Users\SK\Desktop\Citations_Authorea.docx -_Hlk437354082).

Fredriksson, L., Gardner, J.R., Russell, R.S., 1966. Caesium-137. In: Russel, R.S. (Ed.), Radioactivity and Human Diet. Pergamon Press, Oxford, UK, pp. 1–43.

Frissel, M.J., Pennders, R., 1983. Models for the accumulation and migration of ^{90}Sr, ^{137}Cs, ^{239,240}Pu, ^{241}Am in the upper layer of soils. In: Coughtrey, P.J., Bell, J.N.B., Roberts, T.M. (Eds.), Ecological Aspects of Radionuclide Release. Blackwell, Oxford, pp. 63–72.

Hien, P.D., Hiep, H.T., Quang, N.H., Huy, N.Q., Binh, N.T., Hai, P.S., Long, N.Q., Bac, V.T., 2002. Derivation of ^{137}Cs deposition density from measurements of ^{137}Cs inventories in undisturbed soils. J. Environ. Radioact. 62, 295–303.

IAEA, 2009. Quantification of radionuclide transfer in terrestrial and freshwater environments for radiological assessments. In: IAEA-TECDOC-1616. IAEA, Vienna, Austria ISBN 978–92–0–104509–6; www-pub.iaea.org/MTCD/publications/PDF/te_1616_web.pdf (acc. 21.11.2015).

IAEA, 2010. Handbook of parameter values for the prediction of radionuclide transfer in terrestrial and freshwater environments. In: Technical Report Series TR472. International Atomic Energy Agency, Vienna STI/PUB/472; ISBN 92–0–113009–9. www–pub.iaea.org/MTCD/publications/PDF/trs472_web.pdf (acc. 21.11.2015).

Ishikawa, N.K., Uchida, S., Tagami, K., 2008. Distribution coefficients for ^{85}Sr and ^{137}Cs in Japanese agricultural soils and their correlation with soil properties. J. Radioanal. Nucl. Chem. 277, 433–439. http://dx.doi.org/10.1007/s10967-007-7125-z.

Izrael, Y.A., De Cort, M., Jones, A.R., Nazarov, I.M., Fridman, S.D., Kvasnikova, E.V., Stukin, E.D., Kelly, G.N., Matveenko, I.I., Pokumeiko, Y.M., Tabatchnyi, L.Y., Tsaturov, Y., 1996. The Atlas of ^{137}Cs contamination of Europe after the Chernobyl accident, 1-10. http://www.iaea.org/inis/collection/NCLCollectionStore/_Public/31/056/31056824.pdf acc. 7.11.2015.

Kamel, N.H.M., Navratil, J.D., 2002. Migration of ^{134}Cs in unsaturated soils at a site in Egypt. J. Radioanal. Nucl. Chem. 254, 421–429.

Kato, H., Onda, Y., Teramage, M., 2012. Depth distribution of ^{137}Cs, ^{134}Cs, and ^{131}I in oil profile after Fukushima Dai-ichi Nuclear Power Plant accident. J. Environ. Radioact. 111, 59–64.

Kirchner, G., 1998. Applicability of compartmental models for simulating the transport of radionuclides in soil. J. Environ. Radioact. 38, 339–352. http://dx.doi.org/10.1016/S0265-931X(97)00035-0.

Lee, C.J., Chung, C., 1991. Determination of ^{134}Cs in environmental samples using a coincidence gamma ray spectrometer. Int. J. Radiat. Appl. Instrum. Appl. Radiat. Isot. 42, 783–788. http://dx.doi.org/10.1016/0883-2889(91)90211-I.

Lee, M.H., Lee, C.W., 1997. Distribution and characteristics of ^{239,240}Pu and ^{137}Cs in the soil of Korea. J. Environ. Radioact. 37, 1–16. http://dx.doi.org/10.1016/s0265-931x(96)00080-x.

Lettner, H., Bossew, P., Hubmer, A.K., 2000. Spatial variability of fallout ^{137}Cs in Austrian alpine regions. J. Environ. Radioact. 47, 71–82. http://dx.doi.org/10.1016/S0265-931X(99)00023-5.

Li, R., Yang, H., Tang, X., Wu, C., Du, M., 2004. Distribution of ^{137}Cs and organic carbon in particle size fractions in an alumni-haplic acrisol of southern China. Soil Sci. 169, 374–384. http://dx.doi.org/10.1097/01.ss.0000128012.07644.a8.

Likar, A., Omahem, G., Lipoglavšek, M., Vidmar, T., 2001. A theoretical description of diffussion and migration of Cs in soil. J. Environ. Radioact. 57, 42–201. http://dx.doi.org/10.1016/s0265-931x(01)00019-4.

Lujanien, G., Mažeika, K., Šapolait, J., Amulevicius, A., Motiejunas, S., 2006. Kinetics of cesium sorption to clay minerals. Lith. J. Phys. 46, 375–382. http://dx.doi.org/10.3952/lithjphys.46313.

Matsuda, N., Mikami, S., Shimoura, S., Takahashi, J., Nakano, M., Shimada, K., Uno, K., Hagiwara, S., Saito, K., 2015. Depth profiles of radioactive caesium in soil using a scraper plate over a wide area surrounding the Fukushima Dai-ichi Nuclear Power Plant, Japan. J. Environ. Radioact. 139, 46–434. http://dx.doi.org/10.1016/j.jenvrad.2014.10.001.

Mattsson, S., 1975. ^{137}Cs in the reindeer lichen *Cladonia alpestris*: deposition, retention and internal distribution, 1961–1970. Health Phys. 28, 233–248. http://dx.doi.org/10.1097/00004032-197503000-00008.

MEXT, 2011. Ministry of Education, Culture, Sports, Science and Technology. http://www.mext.go.jp/b_menu/shingi/chousa/gijyutu/017/shiryo/_icsFiles/afieldfile/2011/09/02/1310688_1.pdf.

Mishra, S., Arae, H., Sorimachi, A., Hosoda, M., Tokonami, S., Ishikawa, T., Sahoo, S.K., 2014. Distribution and retention of Cs radioisotopes in soil affected by Fukushima nuclear plant accident. J. Soils Sediments 15, 374–380. http://dx.doi.org/10.1007/s11368-014-0985-2.

Mishra, S., Arae, H., Zamostyan, P.V., Ishikawa, T., Yonehara, H., Sahoo, S.K., 2012. Sorption-desorption characteristics of uranium, cesium and strontium in typical podzol soils from Ukraine. Radiat. Prot. Dosim. 152, 238–242. http://dx.doi.org/10.1093/rpd/ncs230.

Monte, L., Brittain, J.E., Håkanson, L., Heling, R., Smith, J.T., Zheleznyak, M., 2003. Review and assessment of models used to predict the fate of radionuclides in lakes. J. Environ. Radioact. 69, 177–205. http://dx.doi.org/10.1016/s0265-931x(03)00069-9.

Mortland, M.M., 1970. Clay-organic complexes and interactions. Adv. Agron. 22, 57–117. http://dx.doi.org/10.1016/s0065-2113(08)60266-7.

Müller, H., Bleher, M., 1997. Exposure pathways and dose calculations in RODOS: improvement of predictions by measured data. Radiat. Prot. Dosim. 73, 61–66. http://dx.doi.org/10.1093/oxfordjournals.rpd.a032164.

Nishihara, K., Iwamoto, H., Suyama, K., 2012. Estimation of Fuel Compositions in Fukushima-Daiichi Nuclear Power Plant. Japan Atomic Energy Agency, JAEA-Data/Code 2012-018, Tokai. Japan.

Poreba, G., Bluszcz, A., Snieszko, Z., 2003. Concentration and vertical distribution of ^{137}Cs in agricultural and undisturbed soils from Chechlo and Czarnocin areas. Geochronometria 22, 67–72.

Putyrskaya, V., Klemt, E., 2007. Modelling ^{137}Cs migration processes in lake sediments. J. Environ. Radioact. 96, 54–62. http://dx.doi.org/10.1016/j.jenvrad.2007.01.017.

Ritchie, J.C., Mc Henry, J.R., 1990. Application of radioactive fallout ^{137}Cs for measuring soil erosion and sediment accumulation rates and patterns: a review. J. Environ. Qual. 19, 215–233. http://dx.doi.org/10.2134/jeq1990.00472425001900020006x.

Roth, K., 2012. Soil Physics. Lecture Notes. Institute of Environmental Physics, Heidelberg University www.iup.uni-heidelberg.de/institut/forschung/groups/ts/students/sp accessed 4 Nov 2014.

Saito, K., Petoussi-Henss, N., 2014. Ambient dose equivalent conversion coefficients for radionuclides exponentially distributed in the ground. J. Nucl. Sci. Technol. 51, 1274–1287. http://dx.doi.org/10.1080/00223131. 2014.919885.

Saito, K., Tanihata, I., Fujiwara, M., Saito, T., Shimoura, S., Otsuka, T., Onda, Y., Hoshi, M., Ikeuchi, Y., Takahashi, F., Kinouchi, N., Saegusa, J., Seki, A., Takemiya, H., Shibata, T., 2015. Detailed deposition density maps constructed by large-scale soil sampling for gamma-ray emitting radioactive nuclides from the Fukushima Dai-ichi Nuclear Power Plant accident. J. Environ. Radioact. 139, 308–319. http://dx.doi.org/10.1016/j.jenvrad.2014.02.014.

Sanada, Y., Torii, T., 2015. Aerial radiation monitoring around the Fukushima Dai-ichi nuclear power plant using an unmanned helicopter. J. Environ. Radioact. 139, 294–299. http://dx.doi.org/10.1016/j.jenvrad.2014.06.027.

Shinonaga, T., Schimmack, W., Gerzabek, M.H., 2005. Vertical migration of ^{60}Co, ^{137}Cs and ^{226}Ra in agricultural soils as observed in lysimeters under crop rotation. J. Environ. Radioact. 79, 93–106. http://dx.doi.org/10.1016/j.jenvrad.2004.05.018.

Smith, J.T., Hilton, J., Comans, R.N.J., 1995. Application of two simple models to the transport of ^{137}Cs in an upland organic catchment. Sci. Total Environ. 168, 57–61. http://dx.doi.org/10.1016/0048-9697(95)04522-3.

Soranzo, A., Epure, E., 2012. Simply Explicitly Invertible Approximations to 4 Decimals of Error Function and Normal Cumulative Distribution Function. http://arxiv.org/pdf/1201.1320v1.pdf.

Southard, R.J., Graham, R.C., 1992. Cesium-137 distribution in a California pelloxerert: evidence of pedoturbation. Soil Sci. Soc. Am. J. 56, 202–207. http://dx.doi.org/10.2136/sssaj1992.03615995005600010031x.

Staunton, S., Dumat, C., Zsolnay, A., 2002. Possible role of organic matter in radiocaesium adsorption in soils. J. Environ. Radioact. 58, 163–173. http://dx.doi.org/10.1016/S0265-931X(01)00064-9.

Steinhauser, G., Brandl, A., Johnson, T.E., 2014. Comparison of the Chernobyl and Fukushima nuclear accidents: a review of the environmental impacts. Sci. Total Environ. 470, 800–817.

Stemmer, M., Hromatka, A., Lettner, H., Strebl, F., 2005. Radiocesium storage in soil microbial biomass of undisturbed alpine meadow soils and its relation to ^{137}Cs soil-plant transfer. J. Environ. Radioact. 79, 107–118. http://dx.doi.org/10.1016/j.jenvrad.2004.04.010.

Takahashi, J., Tamura, K., Suda, K., Matsumura, R., Onda, Y., 2015. Vertical distribution and temporal changes of ^{137}Cs in soil profiles under various land uses after the Fukushima Dai-ichi Nuclear Power Plant accident. J. Environ. Radioact. 139, 351–361. http://dx.doi.org/10.1016/j.jenvrad.2014.07.004.

Tamura, T., 1964. Consequences of activity release: selective sorption reactions of caesium with soil minerals. Nucl. Saf. 5 (3), 262–268.

Teramage, M.T., Onda, Y., Patin, J., Kato, H., Takashi, G., Nam, S., 2014. Vertical distribution of radiocesium in coniferous forest soil after the Fukushima nuclear power plant accident. J. Environ. Radioact. 137, 37–45. http://dx.doi.org/10.1016/j.jenvrad.2014.06.017.

UNSCEAR 1988 Report. Annex, D (1998). United Nation Scientific Committee on the effects of atomic radiation. Sources, Effects and Risk of Ionizing Radiation, Exposures From the Chernobyl Accident, p 3–74, (United Nations, New York., http://www.unscear.org/docs/reports/1988annexd.pdf)

US Environmental Protection Agency (EPA), 1999. Understanding variation in partition coefficient, K_d, values. In: Vol.1, The K_d Model, Methods of Measurement and Application of Chemical Reaction Codes. United States, Office of Air and Radiation. EPA 402-R-99-004A, Washington, DC.

Valcke, E., Cremers, A., 1994. Sorption-desorption dynamics of radiocesium in organic matter soils. Sci. Total Environ. 157, 275–283. http://dx.doi.org/10.1016/0048-9697(94)90590-8.

Van Genuchten, M.T., Wierenga, P.J., 1976. Mass transfer studies in sorbing porous media I. Analytical solutions. Soil Sci. Soc. Am. J. 40, 473–480. http://dx.doi.org/10.2136/sssaj1976.03615995004000040011x.

Winitzki, S., 2008. A Handy Approximation for the Error Function and Its Inverse. A Lecture Note Obtained Through Private Communication.

Wyss, G.D., Jorgensen, K.H., 1998. A User's Guide to LHS: Sandia's Latin Hypercube Sampling Software. SAND98-0210 Sandia National Laboratories, Albuquerque, NM (http://prod.sandia.gov/techlib/access-control.cgi/1998/980210.pdf).

Xu, S., Wörman, A., Dverstorp, B., 2005. Effects of compartmental model structure and long-term inflow pollutograph on model predictions. Radioprotection 40, S477–S483. http://dx.doi.org/10.1051/radiopro:2005s1-070.

Zachara, J.M., Smith, S.C., Liu, C., McKinley, J.P., Serne, R.J., Gassman, P.L., 2002. Sorption of Cs + to micaceous subsurface sediments from the Hanford site, USA. Geochim. Cosmochim. Acta 66, 193–211. http://dx.doi.org/10.1016/S0016-7037(01)00759-1.

Zheng, J., Tagami, K., Bu, W., Uchida, S., Watanabe, Y., Kubota, Y., Fuma, S., Ihara, S., 2014. ^{135}Cs/^{137}Cs isotopic ratio as a new tracer of radiocesium released from the Fukushima nuclear accident. Environ. Sci. Technol. 48, 99–5438. http://dx.doi.org/10.1021/es500403h.